ABSTRACT

Title of Document: LATE MEDIEVAL CLIMATE CHANGES IN THE TROPICAL ATLANTIC AND INTERANNUAL VARIABILITY DOCUMENTED IN NORTHEASTERN CARIBBEAN CORALS

Yuanyuan Xu, Master of Science, 2014

Directed By: Assistant Professor, Kelly Halimeda Kilbourne, Chesapeake Biological Laboratory

Tropical sea surface temperature (SST) has been implicated as a driver of climate changes during the Medieval Climate Anomaly (MCA, 950–1300 CE) but little data exist from the tropical oceans for this time period. I collected multiple *Diploria strigosa* coral colonies from Anegada, British Virgin Islands (18.73°N, 63.33°W) in order to reconstruct climate in the northeastern Caribbean and tropical North Atlantic during the MCA. My Sr/Ca–temperature calibration results derived from three modern *Diploria strigosa* corals suggest that the temperature sensitivity for *Diploria strigosa* is –0.048 (±0.001) mmol/mol°C^{-1}. My reconstruction of MCA climate suggests cooler and wetter conditions in the northeastern Caribbean during the late MCA, indicating that a Pacific La Niña-type climate pattern may have influenced local conditions. Additional analysis indicates that the North Atlantic Oscillation (NAO) was the principal driver of interannual climate variability during the late MCA.

LATE MEDIEVAL CLIMATE CHANGES IN THE TROPICAL ATLANTIC AND INTERANNUAL VARIABILITY DOCUMENTED IN NORTHEASTERN CARIBBEAN CORALS

By

Yuanyuan Xu

Thesis submitted to the Faculty of the Graduate School of the
University of Maryland, College Park, in partial fulfillment
of the requirements for the degree of
Master of Science
2014

Advisory Committee:
Dr. Kelly H. Kilbourne, Chair
Dr. Lee W. Cooper
Dr. Johan Schijf

Acknowledgements

I am grateful for the two years of support for my graduate assistant position that was provided by the National Science Foundation. Fieldwork for this project was accomplished with strong support from the Government of the British Virgin Islands.

I gratefully acknowledge my advisor Dr. Kelly H. Kilbourne for her advice and for working with me throughout the past two years. I also particularly thank my committee members, Dr. Lee Cooper and Dr. Johan Schijf, for their suggestions and support.

Bob Halley, Edgardo Quiñones, and Zamara Fuentes are acknowledged for their significant assistance with fieldwork. Chuan-Zhou Shen, Chris Reich, Jerry Frank, and Sean Pearson contributed during the laboratory phase of my work.

Many thanks also to my classmates Alex Atkinson, Caroline Coulter and Lauren Gelesh for their help with enjoying the graduate life in Southern Maryland. Last but not least, I gratefully thank my dad Yaoquan Xu, my mom Qingzhi Meng, and my younger sister Jiahui Xu for their love and support.

Table of Contents

List of Tables

List of Figures

Chapter 1: Introduction

1.1 Overview

The heat imbalance between Earth's warm tropics and cool poles fundamentally drives its climate system [*Chahine*, 1992]. Much of the energy stored in the climate system resides in the tropics in the form of heat and relatively small changes in the tropics can thus have large impacts on the rest of the climate system [*Hoerling et al*., 2001; *Kerr*, 2001]. For example, the El Niño–Southern Oscillation (ENSO), which is a coupled instability of the ocean–atmosphere system in the tropical Pacific, is associated with seawater temperature variations in the tropical Pacific [*Neelin et al*., 1998], and impacts climate throughout the world on an interannual basis [*Wang et al*., 1999].

Sea surface temperature (SST) variability on seasonal to multidecadal time scales is a key factor controlling climate conditions, such as heavy rains and extreme drought [*Folland et al*., 1986; *Hastenrath and Heller*, 1997; *Spence et al*., 2004]. For example, extreme drought and flood years in northeastern Brazil have been identified from long-term rainfall stations and river discharge data, and are caused by SST variations in the northern tropical Atlantic [*Hastenrath and Heller*, 1977]. Similarly, wet and dry periods in the Sahel region of Africa are strongly related to contrasting patterns of tropical Atlantic SST anomalies between the northern and southern hemisphere that occur over interannual to decadal timescales [*Folland et al*., 1986].

In addition to SST, salinity gradients in the tropics also play an important role in large-scale ocean circulation and global climate change [*Peterson et al*., 2000;

Hoerling et al., 2001]. Fresh water/salt balance in the Atlantic Ocean can impact global thermohaline circulation [*Schmidt et al*., 2004], but more regional effects are also possible; for example, thermohaline circulation can impact the hydrologic balance in the tropical Atlantic [*Zhang and Delworth*, 2005]. *Schmidt et al*. [2004] found evidence for this in foraminiferal records from Caribbean sediment cores that indicated lower Caribbean surface salinity corresponded to warm interglacial periods over the last glacial cycle, presumably as a result of northward migration of the Intertropical Convergence Zone (ITCZ). They hypothesized that millennial-scale salinity anomalies in the Caribbean may have advected into the North Atlantic and impacted North Atlantic deep-water formation. Salinity plays a crucial role in the modern ocean in other regions as well [*Kilbourne et al*., 2004; *Le Bec et al*., 2000; *Li et al*., 2013], for example salinity stratification in the western equatorial Pacific during the generation of ENSO events [*Delcroix et al*., 1998; *Maes et al*., 2000].

Large variations in ocean temperature and salinity may be associated with global or regional climate change. The Intergovernmental Panel on Climate Change (IPCC) Fifth Assessment Report suggests that more extreme temperatures will be commonplace as the global mean temperature increases [*Collins et al*., 2013]. Precipitation may increase in the tropics due to the increase of moisture in the atmosphere [*Trenberth*, 1999]. Based upon theory and high-resolution dynamical models, it has been predicted that the intensity of tropical cyclones will increase and greenhouse warming will shift tropical cyclones towards stronger storms [*Knutson et al*., 2010]. At regional scales, the prediction of climate change is more challenging because other factors, such as local hydrological patterns, urbanization, and land use,

are also significant [*Karl and Trenberth*, 2003]. So temperature and salinity play important roles in predicting large-scale climate change.

Climate records for the past 1000 years can be used to document regional climate patterns and to better understand mechanisms driving climate patterns [*Jones et al*., 2001]. This information can be used to improve predictive models of future climate change. However, abundant, globally distributed instrumental measurements of SST go back only to the late 19th century [*Smith et al*., 2008] and, similarly, salinity measurements are only available beginning in the mid-20th century [*Delcroix et al*., 2005]. In order to understand long-term climate system processes, many natural archives have been used to derive proxy paleoclimate records, including corals, ice cores, tree rings, marine sediment and speleothems [*Esper et al*., 2002; *Giry et al*., 2012; *McDermott*, 2004; *Stansell et al*., 2012; *Yao et al*., 1997].

In this study, I used corals for reconstructing past climate states. Corals contribute to the physical structure of the reefs that develop in tropical and subtropical waters and are widely used for reconstruction of past SST and sea surface salinity (SSS) in tropical areas [e.g., *Giry et al*., 2012; *Swart et al*., 2002]. Coral skeletal material collected from live corals can be used, as well as fossil and sub-fossil corals, provided diagenetic changes in the coral aragonite have not occurred [*Allison et al*., 2007; *McGregor and Gagan*, 2003]. Coral Sr/Ca and stable oxygen isotope composition are SST tracers and they have been widely used in paleotemperature reconstructions [*Corrège*, 2006]. However, the oxygen isotopic composition of coral aragonite is a function of both calcification temperature and the oxygen isotopic composition of seawater. Paired analyses of coral Sr/Ca and $\delta^{18}O$

have been used in the reconstruction of seawater oxygen isotopic composition because the Sr/Ca provides an independent estimate of the water temperature [*McCulloch et al*., 1994; *Gagan et al*., 1998; *Ren et al*., 2002]. In many tropical regions, the oxygen isotopic composition of seawater is linearly related to salinity [e.g., *Fairbanks et al*., 1997; *Watanabe et al*., 2002] and salinity can thus be reconstructed from seawater $\delta^{18}O$ information measurements.

A larger project, of which this thesis is a part, has a focus on SST and SSS variability in the Caribbean during the Medieval Climate Anomaly (MCA, ~900–1300 CE). During previous research efforts on Anegada, British Virgin Islands, several sub-fossil corals were found in an overwash deposit formed around that time period [*Atwater et al*., 2010]. The aims of this thesis are 1) to evaluate the coral Sr/Ca–SST relationship in the coral species *Diploria strigosa* at this site; 2) to assess the coral geochemical response to recent climate and 3) to apply the knowledge of climate recorded in the modern corals at this site to reconstruct climate from a coral that lived during the MCA. A particular focus is on the interannual variability influencing this site. I analyzed the influence of interannual climate variability by using both Sr/Ca and $\delta^{18}O$ in a suite of three modern and one sub-fossil coral cores from Anegada.

1.2 Background

In order to use proxy sources to reconstruct past climate states, it is necessary to fully understand current climate variability and understand potential factors that drive climate change. Knowledge of current climate variability enables the

interpretation of climate signals derived from coral archives. In this section, regional physiographic conditions and modern climatology are explored. The state of knowledge about global and regional climate history of the last millennium is summarized, and background provided on coral-based climate reconstruction.

1.2.1 Physiographic Setting

The samples used in this study are from the island of Anegada, British Virgin Islands (Figure 1). It is an isolated, low-lying island in the northeastern Caribbean Sea (18.73°N, 63.33°W), located about 120 km south of the Puerto Rico Trench, which is located on the plate boundary between the Caribbean Sea and the Atlantic Ocean. The island covers 54 km^2, extending 17 km along a west-to-southeast arc [*Dunne and Brown*, 1979]. Unlike the other volcanic and mountainous islands of the Virgin Islands group, Anegada is nearly flat and consists of limestone, with a maximum elevation of 8.5 m [*Davis and Oldfield*, 2003]. Most of the surface waters surrounding Anegada originate from the tropical Atlantic and enter the Caribbean Sea through several passages including the Anegada passage, which separates the British Virgin Islands from Sombrero Island (British Crown Colony of Anguilla [*Kinder et al*., 1985]).

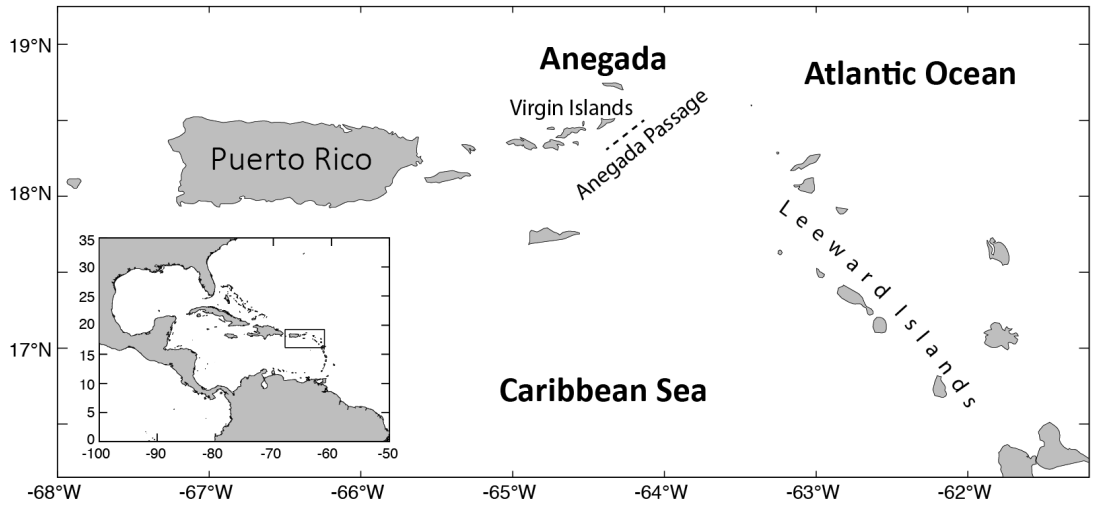

Figure 1. Location of Anegada, relative to the rest of the Virgin Islands, Puerto Rico and the Leeward Islands. The carbonate island lies on the border between the Caribbean Sea and the North Atlantic, along the northern edge of the Anegada Passage, one of only a few deep channels that permit water to flow from the North Atlantic into the Caribbean Sea.

The sub-fossil samples for this project come from an overwash deposit on the island. Recent research on Anegada produced three lines of evidence indicating that seawater washed over low parts of the island a few centuries ago, including several breaches through the sand dunes on the north side of the island. Evidence for these breaches includes the presence of a sand- and shell-dominated sediment sheet that extends at least 0.5 km inland, and limestone boulders and cobbles within that sheet [*Atwater et al.*, 2010]. Some of the large limestone clasts are whole corals that apparently were washed to inland locations by the force of water (Figure 2).

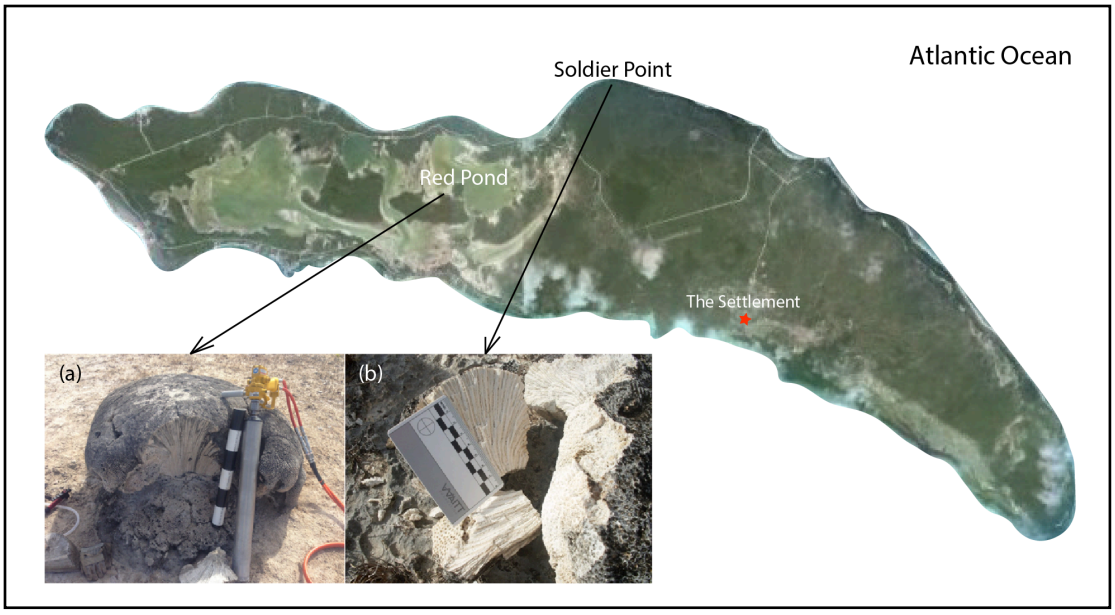

Figure 2. Map of Anegada and pictures of corals found in the overwash deposit. (a) The *Diploria strigosa* coral was found in Red Pond. Black and white striped pattern scale is 10 cm, (b) The *Montastraea cavernosa* coral was found at Soldier Point. The black and white scale is 1 cm.

1.2.2 Climatologic Setting

The climate at Anegada is characteristically tropical. The local SST averages 27.2°C with a 2.8°C annual range in monthly values, derived from NOAA Optimum Interpolation SST (OISST) between 1881 and 2010 (OISST v.2, [*Reynolds et al.*, 2007]). Peak SST occurs in August–October and the lowest SST in January–March (Figure 3). Annual SST variations from Anegada correlate significantly with temperatures over much larger regions (Figures 4 and 5, and Table 1), including the Western Hemisphere Warm Pool (WHWP, a region that combines the Caribbean, Gulf of Mexico and a portion of the eastern Pacific [*Wang and Enfield*, 2001, 2003]), and global combined land-surface and sea-surface temperatures [*Hansen et al.*, 2010]. The strong correlation of Anegada SST to SSTs throughout the northern tropical Atlantic indicates that temperature reconstructions from this site are likely

representative of the region as a whole and therefore can provide valuable information about regional patterns and processes (Figure 5). Additionally, the strong correlation to global temperatures reflects the fact that the tropical Atlantic is an important region to include in global temperature reconstructions.

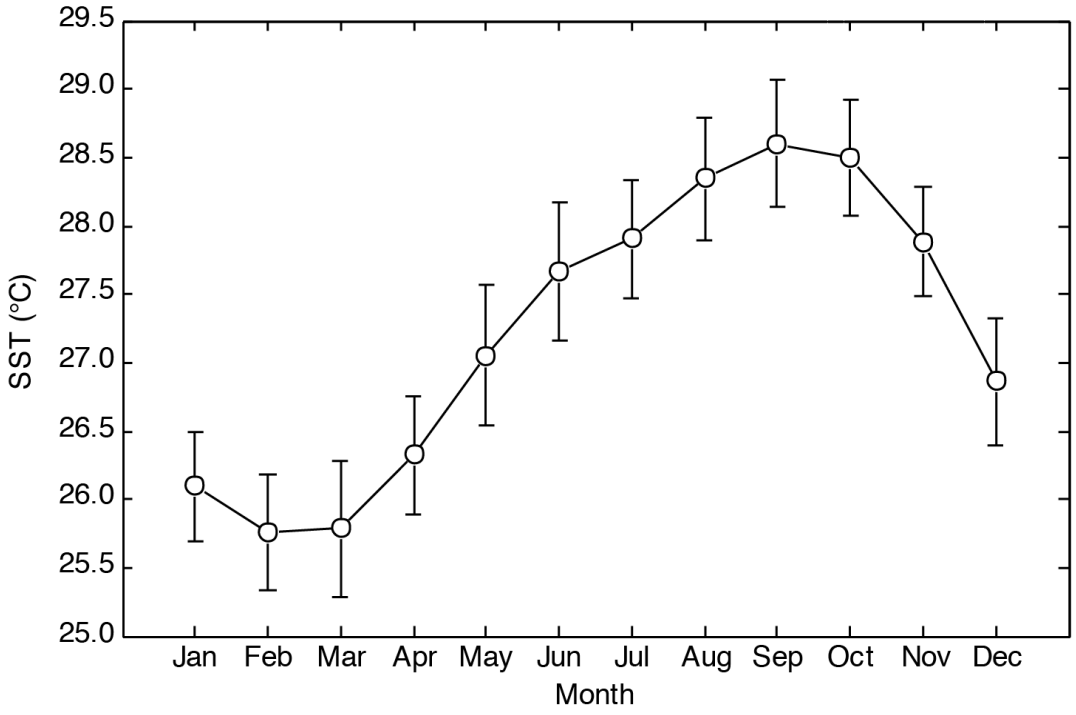

Figure 3. Monthly SST variations in Anegada, BVI from 1881–2010. Data source: OISST v.2 NOAA Optimum Interpolation 0.25-degree daily sea surface temperature [*Reynolds et al.*, 2007].

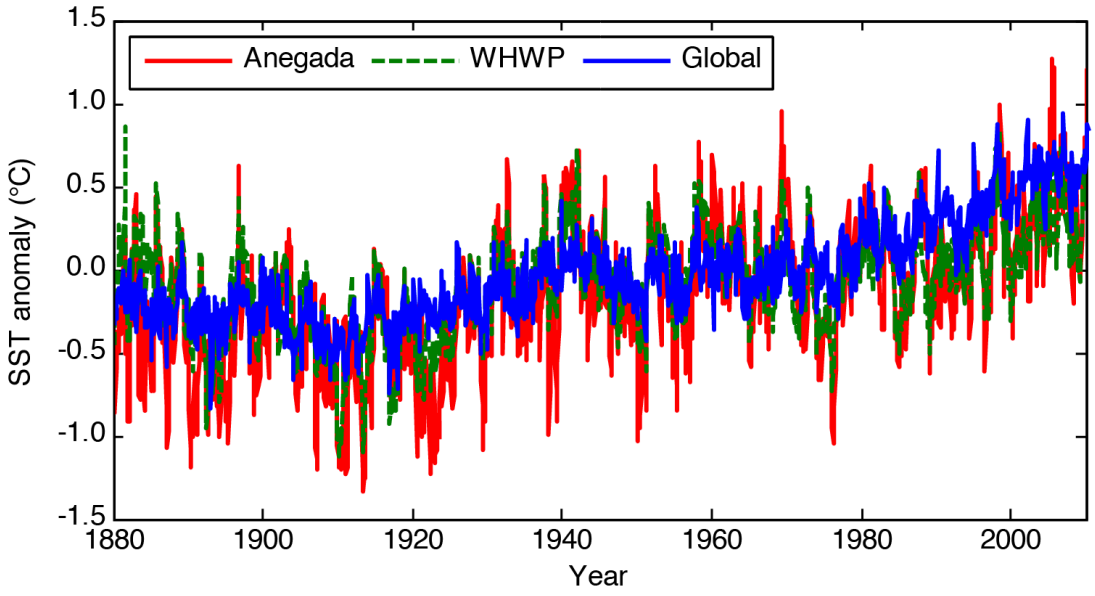

Figure 4. Global, Western Hemisphere Warm Pool (WHWP), and Anegada SST anomalies from 1880 to 2010. Global: Combined land-surface (air) and sea-surface water temperature anomalies (*Hansen et al.*, 2010). WHWP: Extended reconstructed SST (ERSST, [*Smith et al.*, 2008]) data over 7–27°N, 50–110°W, representing the WHWP. Anegada: ERSST data representing Anegada (19°N, 64°W).

Table 1. Correlation coefficients between monthly SST anomalies in Figure 4. All correlation coefficients were calculated over the entire period of overlap (1880–2010 CE) between each data pair and all are significant at the 95% confidence level.

Correlation Coefficient (r)	**Anegada, BVI**	**WHWP**
Global	0.67	0.66
WHWP	0.85	

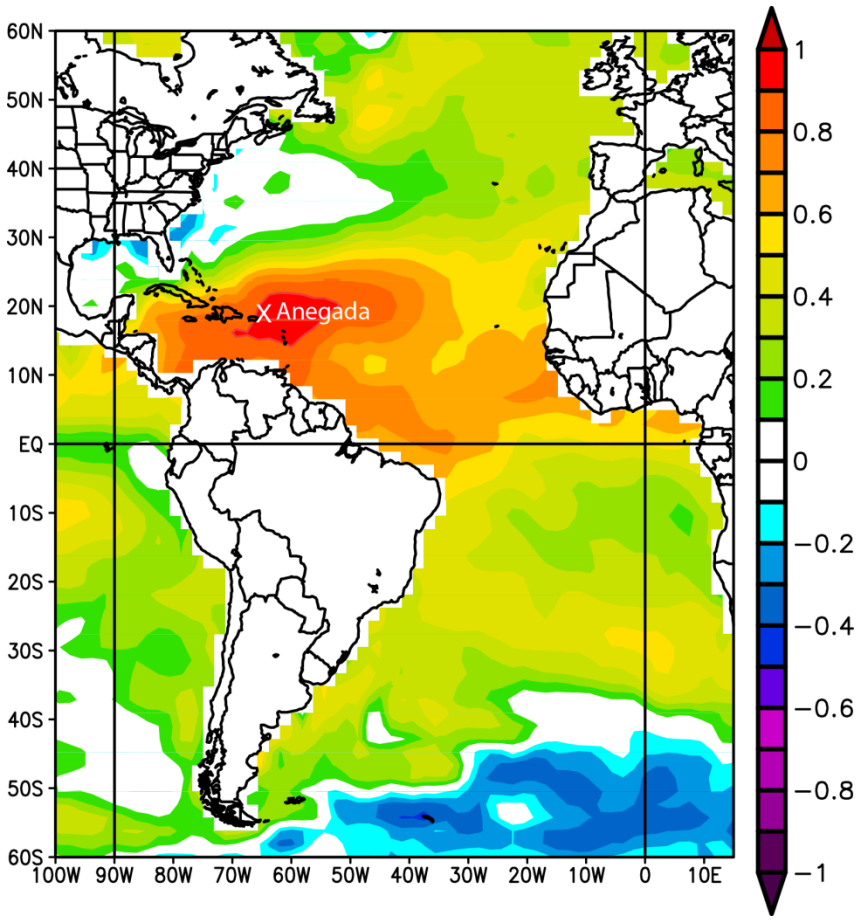

Figure 5. Annual surface temperature 1948–2007 field correlation with annual SST from Anegada (*white X*) from *Smith et al.*, [2008]. Image was provided by the NOAA/ESRL Physical Sciences Division, Boulder Colorado from their interactive data plotting tools at http://www.esrl.noaa.gov/psd/.

Anegada lies between a high-salinity evaporative regime in the subtropical Atlantic and the low-salinity precipitation- and riverine- dominated Caribbean regime to the south [*Dessier and Donguy*, 1994]. According to gridded observing ship data [*Reverdin et al.*, 2007], average SSS from 1970 to 2009 surrounding Anegada from a single grid-box including the study site is 35.7 on the Practical Salinity Scale. The average annual range is 1.2 and the 40 years of salinity data indicate a total range of 1.9, indicating that the seasonal cycle dominates the substantial SSS variability. The

highest salinities occur during March–May and the lowest salinities occur during September–November (Figure 6).

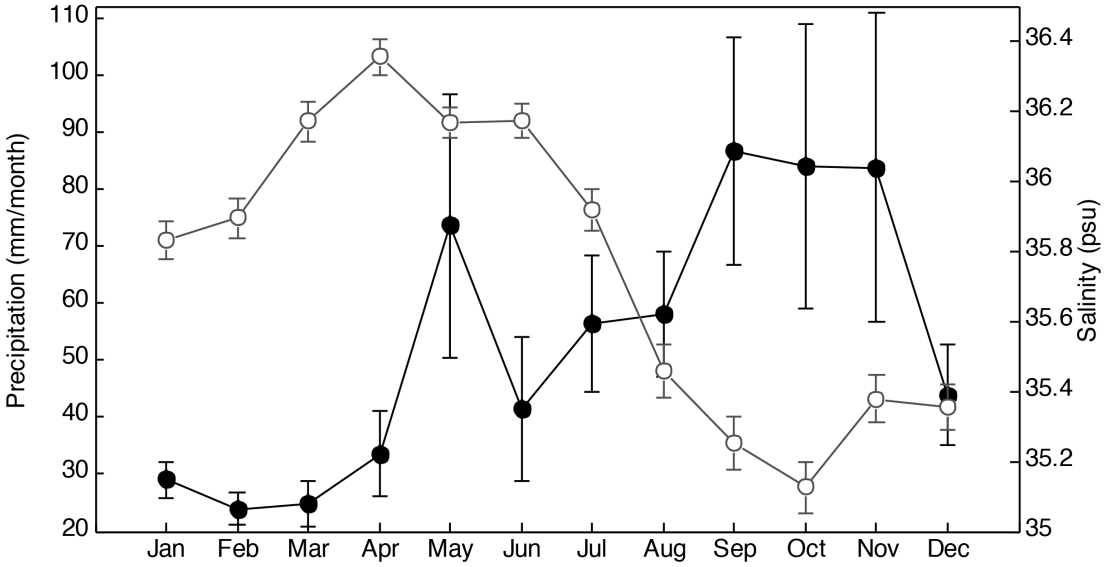

Figure 6. Monthly SSS (open circle) and precipitation (close circle) variations in Anegada, BVI from 1979–2009. Gridded SSS data from a 1°×1° grid box including the study site, Anegada (Laboratoire d'Etudes en Géophysique et Océanographie Spatiales, SSS database in the Atlantic Ocean 50°N–30°S, [*Reverdin et al.*, 2007]). Precipitation data source: GPCP v2.2 combined precipitation data set (combines observations and satellite precipitation data into 2.5°×2.5° global grids, [*Adler et al.*, 2003]).

The variability of salinity is not only affected by local evaporation and precipitation, but also by Caribbean hydrography. The southern Caribbean has abundant fresh water due to the discharge of two major rivers (Orinoco and Amazon) and high rainfall rates due to influence from the Intertropical Convergence zone. From January to July, surface waters from the tropical Atlantic are mixed with fresh water from the Amazon River [*Moore and Todd*, 1993]. From August to December, low salinity lenses that originate in the Orinoco River outflow are usually observed in Caribbean surface waters, because the Orinoco River reaches its maximum flow in

late summer and this freshwater is transported northward [*Müller-Karger et al*., 1989]. As a result, the salinity of southeastern Caribbean surface water is lower than the salinity of tropical Atlantic surface water despite the fact that evaporation usually exceeds precipitation in this area [*Yoo and Carson*, 1990]. Strong easterly trade winds in the region generate northward Ekman transport and bring less salty water from the southern Caribbean northward, creating a salinity front in the northern tropical Atlantic that seasonally approaches Anegada [*Amador*, 1998]. As a result, SSS near Anegada displays variability in response to the migration of the salinity front as it crosses the latitude of the island (Figure 7).

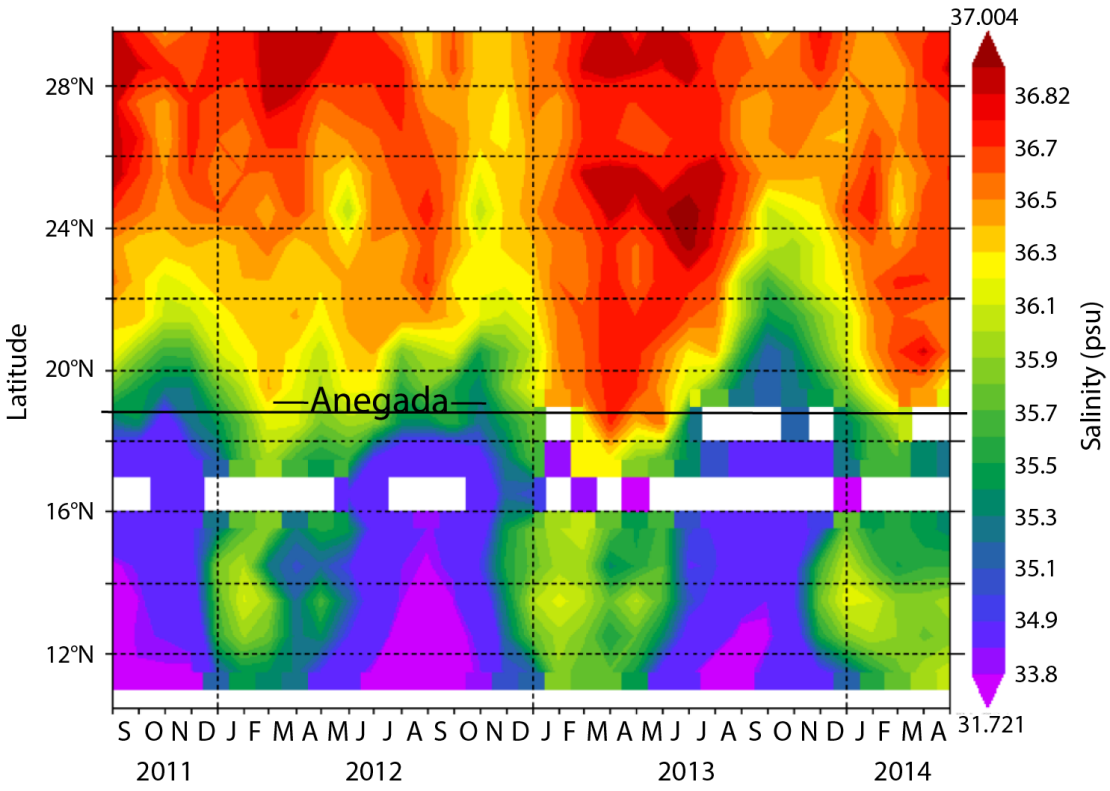

Figure 7. Time/latitude monthly surface salinity at the longitude 63°W–64°W at Anegada (18.73°N, 63.33°W, data from [*Lee et al.*, 2012]) showing migration of the salinity front near Anegada. The solid black line represents the latitude of Anegada. Image was provided by Physical Oceanography Distributed Active Archive Center from their website at http://thredds.jpl.nasa.gov/las/getUI.do.

Precipitation also influences salinity in the region. The seasonal variability of Anegada precipitation is punctuated by two wet seasons: one major rainfall period during September–November and a minor rainfall season in May (Figure 6). In particular, the major rainfall season corresponds to the lowest SSS each year (Figure 6). On interannual time scales, precipitation variability over the Caribbean is associated with the Southern Oscillation [*Rogers*, 1988]. It has been demonstrated that precipitation is generally significantly higher in Low/Wet modes of the Southern Oscillation than in High/Dry modes [*Rogers*, 1988].

The usual patterns of climate in the Caribbean and northern tropical Atlantic described above are perturbed over interannual time scales by three main patterns of variability: ENSO, North Atlantic Oscillation (NAO) and Tropical Atlantic Variability (TAV) [*Cazja et al*., 2002; *Marshall et al*., 2001]. The NAO is a major source of interannual climate variability, governed by the oscillation of atmospheric mass between higher latitudes near Iceland and the subtropical Atlantic [*Visbeck et al*., 2001]. The NAO index is defined by the difference in sea-level atmospheric pressure between the Azores high and Icelandic low [*Hurrell*, 1995]. The NAO is most active from December to March [*Marshall et al*., 2001] and influences SST in the Caribbean during the spring [*Czaja et al*., 2002]. In general, there is a negative correlation between the strength of the pressure gradient associated with the NAO and precipitation in the northeastern Caribbean [*Malmgren et al*., 1998]. Wintertime precipitation in the northern tropical Atlantic is especially associated with NAO shifts, which exert their influence by affecting northern tropical Atlantic trade winds [*George and Saunders*, 2001].

ENSO is a coupled instability of the ocean-atmosphere system in the tropical Pacific but has global impacts [*Neelin et al*., 1998; *Wang et al*., 1999]. Like the NAO, ENSO is phase-locked to the seasonal cycle and generally has its maximum in the Northern Hemisphere winter. *Czaja et al*. [2002] determined that almost all northern tropical Atlantic SST extreme events in the recent 60 years can be related to either ENSO or NAO based on a spring SST index. *Wang et al*. [2008] reported that the Western Hemisphere Warm Pool size and intensity are modulated by ENSO on interannual timescales. Generally, the northern tropical Atlantic is warmer in spring

after El Niño years [*Wang*, 2002]. ENSO events also affect changes in storm tracks in the Caribbean region and produce significant seasonal anomalies in precipitation, such as wet winters and dry summers [*Ropelewski and Halpert*, 1987]. In particular, ENSO has the greatest impact on Caribbean rainfall during August–October (the late rainfall season) and November–January (the early dry season) [*Hu and Huang*, 2007].

The TAV is interactive with other climate variability, especially ENSO and NAO [*Xie and Carton*, 2004]. It is a fluctuation of north-south and east-west SST gradients and SST-driven fluctuations in the trade winds [*Marshall et al*., 2001] and, like ENSO and NAO, it is strongly connected to the seasonal cycle [*Xie and Carton*, 2004]. The early rainfall season in Anegada is associated with TAV because the Atlantic ITCZ, where the northeast and southeast trade winds meet in the tropical Atlantic, shows a tendency to shift northward and increase precipitation in the northern tropical Atlantic [*Xie and Carton*, 2004]. TAV has the greatest impact on Caribbean rainfall from May to July (the early rainfall season) [*Hu and Huang*, 2007].

In addition, SSS in the tropical Atlantic is indirectly influenced by ENSO and TAV via the variability of trade winds [*Stramma and Schott*, 1999]. The strength of wind-driven currents over the tropical Atlantic affects the migration of surface salinity in Anegada by influencing the freshwater lenses to the south and salty water incursions from the north [*Chérubin and Richardson*, 2007]. Trade winds are weak in the western tropical Atlantic during El Niño and are strong during La Niña [*Stramma and Schott*, 1999]. The location of the ITCZ, which is related to TAV, influences the zonal wind and wind-induced evaporation [*Xie and Carton*, 2004].

1.2.3 Coral-based Climate Reconstructions

Corals are ideal proxies for studying tropical climate variability because they grow ubiquitously in the tropics [*Corrège*, 2006]. They can live for centuries and their relatively high growth rates permit monthly sampling that can resolve seasonal to interannual variability [*Highsmith*, 1979]. The age of a piece of coral can be precisely determined by U-series radiometric dating, providing good age control [*Broecker and Thurber*, 1965]. *Shen et al.* [2008] showed that high-precision U–Th dating yields an age uncertainty of only ± 0.2–0.3 years for modern corals using 1–2 g sub-samples. In addition, the annual density bands provide internal age control [*Hendy et al.*, 2003]. In combination with the U-series dating, the age of every annual density band can be precisely determined.

The geochemistry of coral skeletal material can provide surface temperature and salinity information [*Corrège*, 2006]. A simple inverse linear relationship has been observed between coral Sr/Ca ratios and ambient temperatures [*Smith et al*., 1979]. Based upon this observation, coral Sr/Ca ratios have been widely used to reconstruct seawater temperature [e.g., *McCulloch et al*., 1994; *Swart et al*., 2002; *Goodkin et al*., 2005]. The Sr/Ca ratio in slow-growing corals (<5 mm/year) may also be influenced by skeletal growth rates [*de Villiers et al*., 1994; *Goodkin et al*., 2005], but the influence of growth rate on coral Sr/Ca ratio is weak in fast-growing corals and the coral Sr/Ca ratio is still considered a "clean" temperature proxy that is primarily affected by seawater temperature [*Hirabayashi et al*., 2013].

Coral $\delta^{18}O$, which is the deviation of coral skeletal $^{18}O/^{16}O$ relative to the $^{18}O/^{16}O$ of a standard, also records temperature, but it can be a more complex proxy

of SST because it also records information on the isotopic composition of the seawater [*Gagan et al*., 2000; *Weber and Woodhead*, 1972]. In the modern tropical ocean the seawater isotopic composition of seawater is often linearly related to salinity [*Fairbanks et al*., 1997; *Watanabe et al*., 2002]. Paired analyses of coral Sr/Ca and $\delta^{18}O$ have been applied to extract the temperature component in coral $\delta^{18}O$ and reconstruct salinity [*Cahyarini et al*., 2008; *Gagan et al*., 1998; *McConnell et al*., 2009; *McCulloch et al*., 1994]. In this study, I used this same approach with corals collected from Anegada to determine paleoclimate information.

Chapter 2: Modern Coral Study

2.1 Introduction

A few key genera of reef-building corals are used in most paleoclimate studies to reconstruct tropical climate [*Corrège*, 2006; *DeLong et al.*, 2007; *Saenger et al.*, 2008]. *Porites* is the genus most commonly used in the Pacific [e.g., *Corrège*, 2006; *Gagan et al.*, 2012; *McGregor and Gagan*, 2003; *Shen et al.*, 1996]. In the Atlantic region, *Montastrea* is the genus most successfully used in paleoclimate studies [*Kilbourne et al.*, 2008; *Saenger et al.*, 2008; *Swart et al.*, 2002; *Watanabe et al.*, 2001; *Watanabe et al.*, 2002].

Another common coral genus on Atlantic reefs is *Diploria*, which has been studied for paleoclimate much less extensively. Work on the genus *Diploria* has included specimens of the species *D. labyrinthiformis* from Bermuda where a strong impact of coral growth on geochemistry in slow-growing specimens was observed [*Cohen et al.*, 2004; *Goodkin et al.*, 2005]. Many researchers discounted using the genus for paleoclimate reconstructions based upon this work. However, *Hetzinger* [2006] evaluated fast-growing specimens of the species *D. strigosa* from Guadeloupe, in the eastern Caribbean, for paleoclimate studies and found it to be a promising archive. Further work on *D. strigosa* from the southern Caribbean showed that a Sr/Ca–SST calibration based on monthly mean data is similar to prior work and that seasonality and interannual to inter-decadal SST variability is well documented by Sr/Ca records in this species [*Giry et al*., 2012].

Slopes in coral Sr/Ca–SST linear calibration equations are similar for a given genus but show considerable variability among genera [*Corrège*, 2006; *Weber*, 1973]. These results have been accepted by the scientific community, with different researchers publishing individual calibrations for different genera [e.g., *Corrège*, 2006; *Gallup et al.*, 2006; *Maupin et al.*, 2008; *Swart et al.*, 2002]; I extend this work here for *D. strigosa*.

Many previous calibration studies [*Hetzinger et al.*, 2006; *Shen et al.*, 1996] have defined the slope using single coral colonies, but *Goodkin et al.* [2007] pointed out that multi-colony calibrations are inherently more accurate for paleoclimate reconstructions than those that use individual coral specimens selected from a random population of a particular species. In this study, I develop calibration slopes from multiple modern corals to provide a more robust relationship for this species.

However, a complicating factor for multi-colony calibrations is that differences in mean Sr/Ca values have been found in corals growing on the same reef at the same time that seem unrelated to temperature [*Giry et al.*, 2012; *Pfeiffer et al.*, 2008]. My study uses two approaches to compensate for potential mean shifts with Sr/Ca data from three colonies. The approaches are to (1) center the data before regression by removing the mean Sr/Ca value of each coral colony and removing the mean SST value; (2) regress using the Sr/Ca and SST anomalies i.e., remove the average annual cycle in Sr/Ca and SST time series.

Most prior calibration studies used the Ordinary Least Squares (OLS) regression technique, which has been shown to have limitations [*Solow and Huppert*, 2004]. In this study, I explore the use of OSL and compare it to other methods that

have been recommended as alternates, such as Reduced Major Axis (RMA) regression [*Quinn and Sampson*, 2002] and Weighted Least Squares [*Thirumalai et al.*, 2011]. OLS is a generalized linear modeling technique that regresses a response variable on a predictor variable [*Cavalli-Sforza and Edwards*, 1967]. This technique minimizes the sum of squared vertical distances between the observed response variables and the predicted variables [*Cavalli-Sforza and Edwards*, 1967]. RMA is also a least-squares method but differs from OLS in that it uses a different definition for the residuals. It accounts for potential errors in both variables simultaneously by minimizing the distance perpendicular to the regression line [*Clarke*, 1980].

The primary difference between OLS and RMA is that RMA assumes equal error variances exist in both the dependent variable and the independent variable, while OLS only accounts for errors in the dependent variable [*Smith*, 2009]. For OLS and RMA, the resulting difference in regression lines is that OLS regression lines are asymmetric, i.e., dependent on which variable is on the x-axis. However, the RMA regression lines are symmetric with respect to inversion of the axes. *Solow and Huppert* [2004] pointed out that OLS regressions produce a biased estimate of SST due to the presence of errors in SST used in the calibration. They recommended a bias correction, but to best of my knowledge, no studies have yet incorporated such a correction.

Fitch and Margoliash [1967] suggested the Weighted Least Squares (WLS) method to utilize the errors in both independent and dependent variables for regressions in general and *Thirumalai* [2011] wrote MATLAB ® code to implement WLS as described in *York et al*. [2004]. In this technique, each term includes an

additional weight, determining how much each observation in the data set influences the final parameter estimates. Less weight is given to the less precise measurements and more weight to more precise measurements. In most studies, errors are based on assumptions about the distribution of the data [*Bevington and Robinson*, 1969; *Huber et al.*, 2002]. Here, as an example, I use a bootstrap method with weighted least squares (BWLS) to iteratively determine the range of calibrations possible from a given dataset.

This study builds upon the initial studies of *D. strigosa* as a paleoclimate archive. I used three modern corals to develop calibrations based on centered Sr/Ca data and anomalies. Furthermore, four calibration techniques (OLS, RMA, WLS, and BWLS) are used to assess how assumptions in different methods influence the calibrations and provide a best estimation for this coral species.

2.2 Data and Methods

2.2.1 Sampling

The coral samples used in this study were collected as hand samples in March 2013 from the beach berm at Soldier Point, Anegada (Figure 2). The pristine-looking coral boulders collected were originally thought to have been washed onto the beach by Hurricane Earl in 2010, based on previous observations at this site soon after the hurricane [*Atwater et al.*, 2014], but our dating results indicate they likely washed ashore in winter storms.

Approximately 5 cm diameter cores were drilled from each of the three coral boulders in the field. The cores were designated 13AN17, 13AN18, 13AN19 and

were cut along the growth direction into approximately 5 mm thick slabs using a tile saw. Each slab was individually immersed in a clean plastic container with deionized water and ultrasonicated for 30 minutes. Following a rinse in deionized water, the samples were air-dried and stored covered with clean Kimwipes®.

Coral slabs were drilled using a computer-controlled micromilling system, equipped with a 0.5-mm diameter carbide steel dental drill bit. Before drilling coral slabs, coral extension rates were estimated by measuring the distance between ten banded couplets. The targeted sampling resolution was 12 samples per year. Sub-samples of skeletal powder were extracted carefully at constant sampling depths (0.5 mm per sub-sample) along the center of the thecal wall, to obtain the best chronology and environmental signal possible [*Giry et al*., 2010].

2.2.2 Coral Sr/Ca

Sr/Ca ratios in the coral aragonite were measured using a Perkin Elmer Optima 8300 Inductively Coupled Plasma Optimal Emission Spectrometer (ICP-OES) at Chesapeake Biological Laboratory. I weighed 150 ± 50 μg coral powder from each sample and dissolved it in different volumes (2–4 mL) of 2% trace metal grade nitric acid to bring the concentration of calcium to ~20 ppm. Calibration standards with known calcium and strontium concentrations were used to convert instrumental signal intensity to sample concentration. Reference standards were added after each sample to calculate an instrumental drift correction to be applied to the data, as per *Schrag* [1999]. The calcium and strontium concentrations of the reference standards were similar to the samples, with values of ~20 ppm and 400 ppb, respectively. An in-house laboratory coral standard prepared from *Orbicella*

faveolata [*Budd et al.*, 2012] dissolved in 2% nitric acid to similar calcium concentration as the samples was used as an independent check of analytical precision and accuracy. Long-term analytical precision for the reference standard solution is 0.12% (2σ, 0.011 mmol-Sr/mol-Ca, n = 4475). Long-term analytical precision for the coral standard solution is 0.26% (2σ; 0.023mmol-Sr/mol-Ca, n = 578). Applying a Sr/Ca–temperature relationship of 0.042 mmol $mol^{-1}°C^{-1}$ from *Hetzinger* [2006] to the 2σ standard deviations of the reference and coral solutions results in estimated temperature standard errors on individual data points of 0.26°C and 0.55°C for reference standard solution and coral standard solution, respectively.

2.2.3 Coral Chronology

In this study, the age of the corals was determined by a combination of uranium-series dates, X-radiographs, and correlations of coral Sr/Ca to SST. Sub-samples weighing on average 600 ± 200 mg and representing approximately one year of coral growth were cut from coral slabs 13AN17 and 13AN18. Note that we compared Sr/Ca measured in coral 13AN19 with the values measured in coral 13AN17 to determine the age of 13AN19. Uranium-series analysis was undertaken on these sub-samples at the High-Precision Mass Spectrometry and Environment Change Laboratory at National Taiwan University. The wet chemistry was performed following *Shen et al.* [2003] and instrumental analysis was performed by Multicollector-Inductively Coupled Plasma-Mass Spectrometry (MC-ICP-MS) using the method of *Shen et al*. [2012].

X-radiographs taken at the United States Geological Survey in St. Petersburg, Florida, were used to reveal the annual density band couplets for age modeling. The

positions of the dated coral pieces were identified on the X-radiographs and an initial depth/age relationship determined by annual density band counting from the position and date indicated. The conversion of the Sr/Ca data from depth domain to time domain was achieved by matching coral Sr/Ca seasonal cycles to SST seasonal cycles using AnalySeries software (available through NOAA's National Climate data center at http://www.ncdc.noaa.gov/data-access/paleoclimatology-data/datasets/software) [*Paillard et al*., 1996]. The SST record used for alignment is the 2° × 2° gridded Extended Reconstructed Sea Surface Temperature (ERSST) version 3b data [*Smith et al*., 2008] centered on 19°N, 64°W. The time domain Sr/Ca ratios were re-sampled to monthly intervals to be able to compare with even-monthly SST time series data. Annual growth rates were calculated from two successive winters in each annual cycle as defined by the depth-domain Sr/Ca data.

2.2.4 Instrumental Data

National Oceanic and Atmospheric Administration/National Climatic Data Center (NOAA/NCDC) ERSST v.3b [*Smith* et al., 2008] is the major data source I used for the instrumental SST data to calibrate Sr/Ca ratios in my samples. The temporally and spatially complete ERSST data were created by interpolating between gaps in the instrumental database [*Smith and Reynolds*, 2004]. Satellite SST data and local buoy data (from NOAA) were also considered, but their temporal coverage is limited and the data did not extend back to the earliest years represented in coral 13AN18.

2.2.5 Statistical Methods

Previous work exploring the potential for the species *D. strigosa* to serve as a paleoclimate archive found significant correlations of skeletal Sr/Ca and $\delta^{18}O$ to SST and used an ordinary least squares regression to quantify the Sr/Ca–SST and $\delta^{18}O$–SST relationships [*Hetzinger et al.*, 2006]. For the OLS regression performed here, the estimated error of the slope equals the ratio of standard error of the regression and the square root of the total sum-of-squares in instrumental temperatures. The standard error of the slope of the RMA regression was estimated following *Davis* [2002].

In order to evaluate the OLS and RMA regressions, I used a more efficient estimator weighted least squares, which minimizes the weighted sum-of-squares, accounting for estimated errors in both dependent and independent variables [*Fitch and Margoliash*, 1967]. The slope, intercept, and standard error of this regression were calculated following *York et al.* [2004] using the MATLAB code provided in *Thirumalai et al.* [2011].

Furthermore, the BWLS technique gives me a view of the range of regression lines that can be obtained from the regression data and allows me to estimate how potential outliers affect the calibrations. In the BWLS technique, 75% of the data were randomly selected 1000 times and each selection was analyzed by using the WLS technique [*York et al.*, 2004]. Each random selection leaves out 25% of the data that can be used to evaluate the calibration. In contrast to the errors for OLS, RMA, and WLS, which are calculated from a single calibration, the BWLS calibration

technique uses the 1000 WLS regression slopes to estimate the 95% confidence interval on the value of the regression slope.

2.3 Results

2.3.1 Age Model

The initial geochemistry data are relative to depth and were converted to monthly data to determine the Sr/Ca–temperature dependence as described above. The re-sampled monthly even time series data are similar to the age-modeled raw data (Figure 8). All following analyses are based on the monthly even time series data. Depth-domain Sr/Ca ratios match with annual density bands, with periods of maximum Sr/Ca ratios corresponding to low-density bands and minimum Sr/Ca ratios corresponding to high-density bands (Figure 9). The initial age model step produces data that are organized in relative time, but lack a firm date for each sample because of the uncertainty in the U-series dates for each sample. Uranium-series dates show that the age for the dated portion of the skeleton 13AN17 and 13AN18 (Figure 9) are 1989.5 ± 0.58 CE and 1953.3 ± 0.72 CE, respectively. Correlating the Sr/Ca anomalies to SST anomalies over a range of time lags around the U-series uncertainty provides a way to determine a best estimate for the age of each sample (Figure 10 and Table 2).

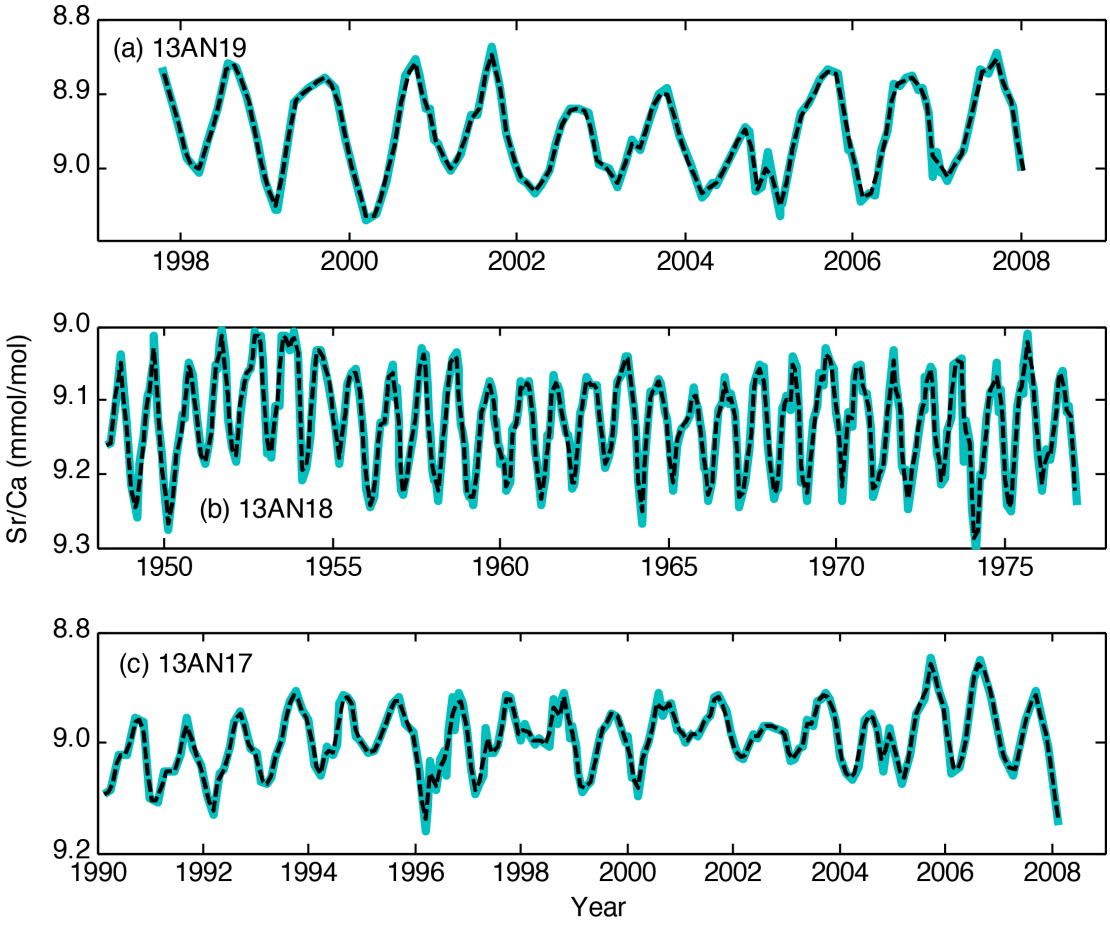

Figure 8. Comparison of the age-modeled raw Sr/Ca data and the re-sampled time series data in modern corals. The solid green lines represent age-modeled raw Sr/Ca data. The dashed black lines represent the re-sampled Sr/Ca data. The re-sampled lines are smoother than the age-modeled raw data lines, but generally have a similar pattern of variance.

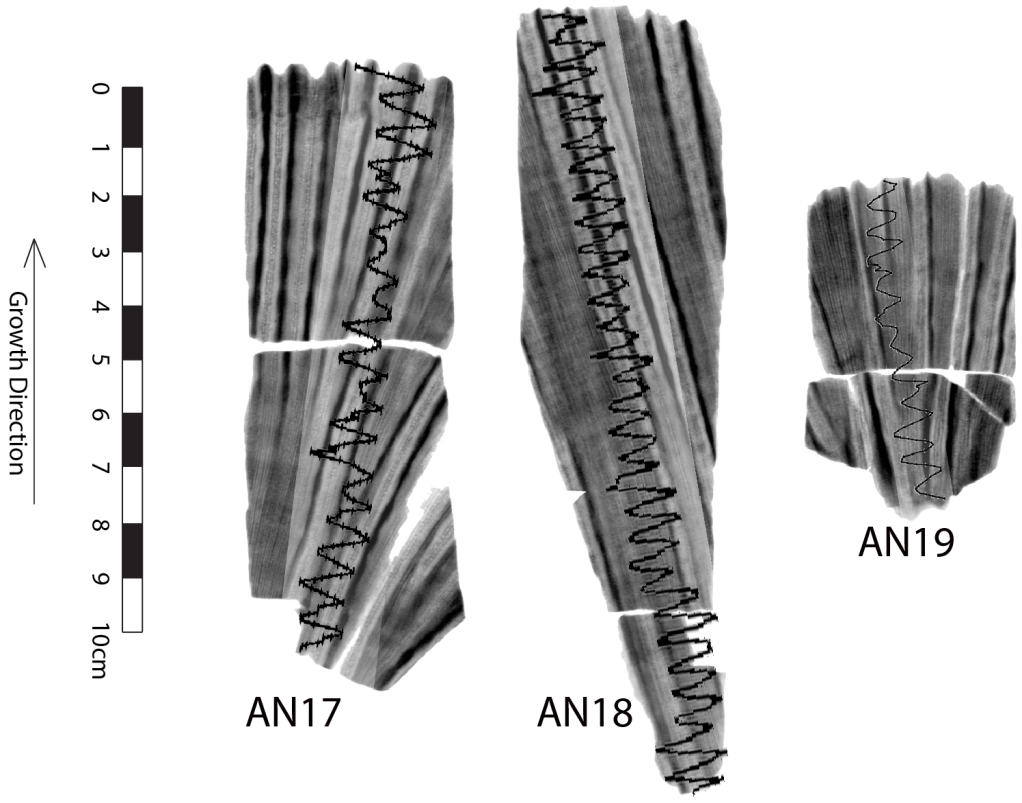

Figure 9. Coral Sr/Ca ratios on X-radiographs. Low Sr/Ca values (toward the right), indicating higher temperatures, correspond to the high-density bands in the X-radiographs.

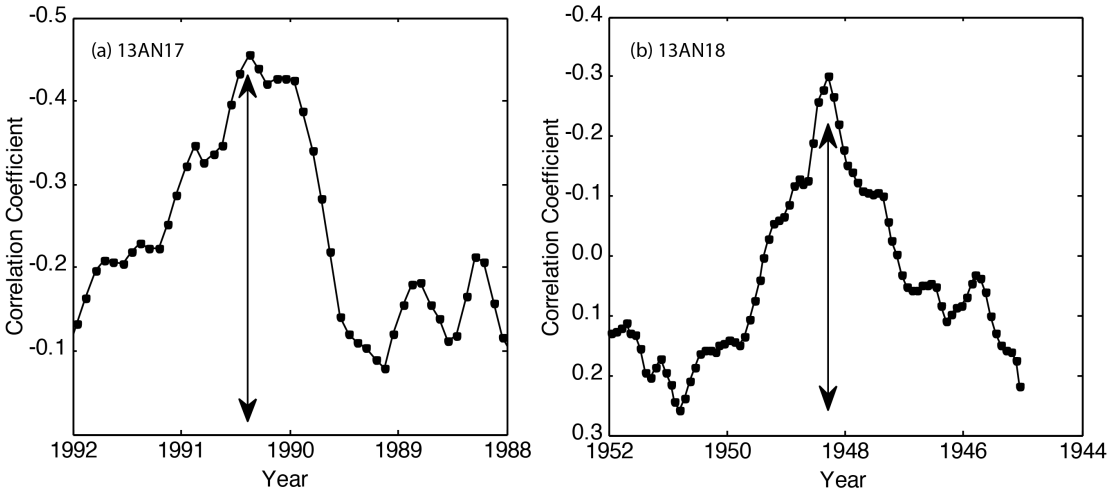

Figure 10. Lagged correlation of Anegada SST anomalies with coral Sr/Ca anomalies. The dates corresponding to the minimum correlation value were designated the start date if the coral.

Table 2. Ages of modern corals.

Coral colony	Start date	End date	Time span
13AN17	Winter, 1990	Winter, 2008	18 years
13AN18	Spring, 1948	Winter, 1977	29 years
13AN19	Summer, 1997	Winter, 2008	10.5 years

2.3.2 Calibration of Sr/Ca with SST

Calibration slopes obtained from Sr/Ca–SST regressions on three modern corals using four different methods are often statistically different from each other, but are within a relatively narrow range of slopes compared to the range of Sr/Ca–SST slopes reported in the literature. Table 3 summarizes the linear regression equations between the mean-centered Sr/Ca time series and ERSST data. In each single coral colony, OLS regression is the same as the WLS and BWLS regressions (Figure 11). The slope of the RMA regression in each coral colony is different from those determined with other regression techniques. Similarly, when the data from all

three corals are centered and combined, the ordinary least squares and weighted least squares give the same results, but the RMA regression is significantly different.

Table 3. Summary of linear regression equations between the removed-average Sr/Ca time series and ERSST data in modern corals. Note that the regression equation for the BWLS technique represents the average of all bootstrap regressions.

Coral core	Regression equation
AN17	
OLS	Sr/Ca = –0.043(±0.003)×SST
RMA	Sr/Ca = –0.053(±0.002)×SST
WLS	Sr/Ca = –0.043(±0.002)×SST
BWLS	Sr/Ca = –0.043(±0.002)×SST
AN18	
OLS	Sr/Ca = –0.052(±0.002)×SST
RMA	Sr/Ca = –0.059(±0.002)×SST
WLS	Sr/Ca = –0.052(±0.001)×SST
BWLS	Sr/Ca = –0.052(±0.002)×SST
AN19	
OLS	Sr/Ca = –0.047(±0.002)×SST
RMA	Sr/Ca = –0.053(±0.002)×SST
WLS	Sr/Ca = –0.047(±0.002)×SST
BWLS	Sr/Ca = –0.047(±0.002)×SST
All	
OLS	Sr/Ca = –0.048(±0.001)×SST
RMA	Sr/Ca = –0.056(±0.001)×SST
WLS	Sr/Ca = –0.048(±0.001)×SST
BWLS	Sr/Ca = –0.048(±0.001)×SST

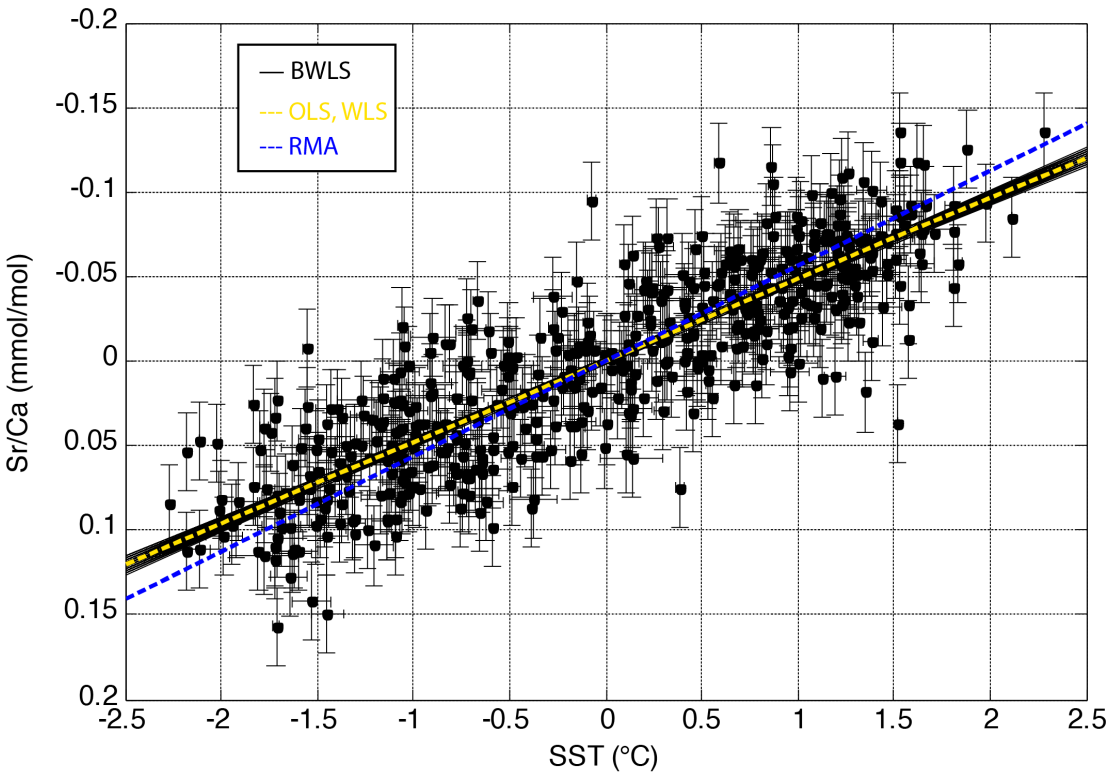

Figure 11. Regressions lines by applying OLS, RMA, and WLS techniques to removed-average Sr/Ca and removed-average ERSSTs. The black points with error bars (2SE) represent data points in all three coral cores.

A weakness of calibrating monthly mean-centered Sr/Ca data to SST is that the regression results are strongly controlled by the seasonal cycle [*Crowley et al.*, 1999; *DeLong et al.*, 2007]. To get around this issue, repeated the regression analysis on the Sr/Ca and SST monthly anomalies. Sr/Ca anomalies are significantly correlated with SST anomalies in all modern corals ($p < 0.001$, Table 4). Table 5 summarizes linear regression equations between Sr/Ca anomalies and ERSST anomalies. The slopes in OLS regressions are only slightly different from the slopes in WLS and BWLS regressions (Figure 12). Similar to the previous set of regressions on mean-centered data, the slopes of the RMA regressions are higher than the slopes

of the other regressions. The large difference in regression equations shows the importance of assumptions about the distribution of error in the data when the signal-to-noise ratio is small as is the case with the monthly anomaly data.

Table 4. Correlation coefficients between Sr/Ca anomalies and ERSST temperature anomalies in modern corals demonstrate the significant relationship between Sr/Ca and temperature at this site.

	AN17	**AN18**	**AN19**	**All**
Correlation coefficients (r)	–0.44	–0.30	–0.53	–0.38
p-value	<0.001	<0.001	<0.001	<0.001
Number of data points (N)	217	347	214	688

Table 5. Linear regression equations between Sr/Ca anomalies and ERSST anomalies. Note that the regression for BWLS represents the average of all bootstrap regressions.

Coral core	**Regression equation**
AN17	
OLS	Sr/Ca = –0.043(±0.006)×SST
RMA	Sr/Ca = –0.098(±0.006)×SST
WLS	Sr/Ca = –0.046(±0.005)×SST
BWLS	Sr/Ca = –0.046(±0.007)×SST
AN18	
OLS	Sr/Ca = –0.025(±0.004)×SST
RMA	Sr/Ca = –0.081(±0.004)×SST
WLS	Sr/Ca = –0.026(±0.004)×SST
BWLS	Sr/Ca = –0.026(±0.005)×SST
AN19	
OLS	Sr/Ca = –0.051(±0.007)×SST
RMA	Sr/Ca = –0.097(±0.007)×SST
WLS	Sr/Ca = –0.052(±0.007)×SST
BWLS	Sr/Ca = –0.052(±0.007)×SST
All	
OLS	Sr/Ca = –0.034(±0.003)×SST
RMA	Sr/Ca = –0.089(±0.003)×SST
WLS	Sr/Ca = –0.036(±0.003)×SST
BWLS	Sr/Ca = –0.036(±0.004)×SST

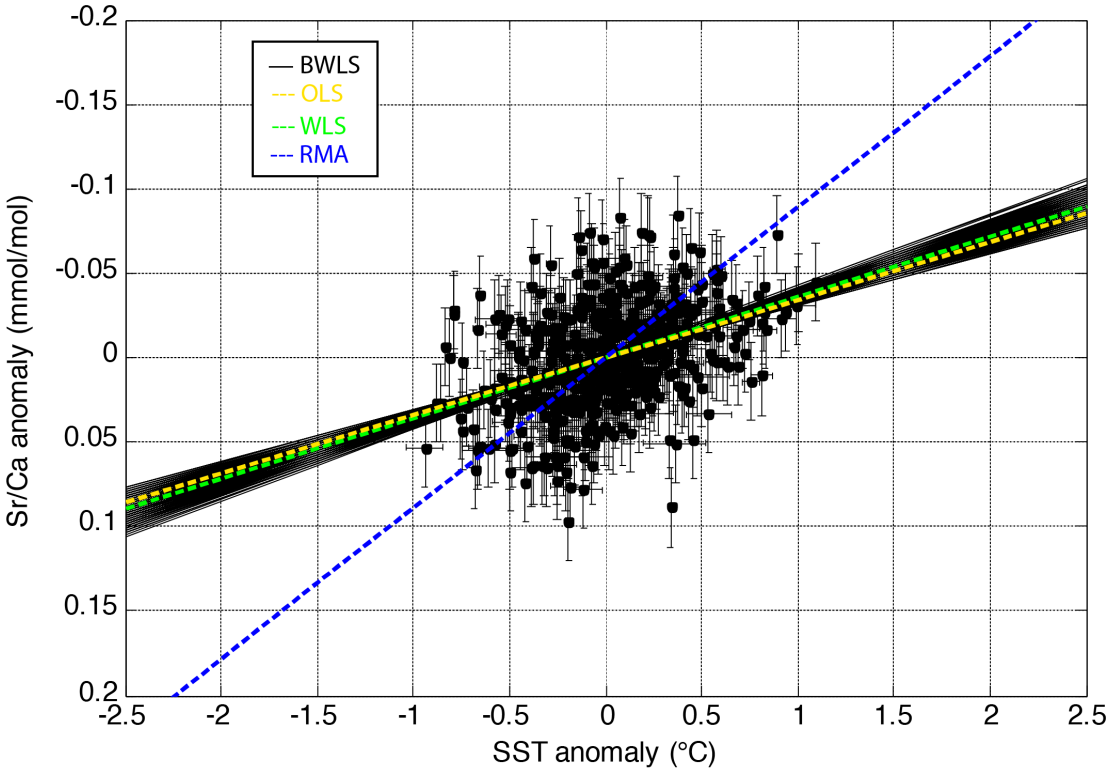

Figure 12. Regressions lines by applying OLS, RMA, and WLS techniques to Sr/Ca anomalies and ERSST anomalies. The black points with error bars (2SE) represent data points in all three coral cores.

2.3.3 Coral Skeletal Growth Rate and Coral Sr/Ca Means

Coral growth rates have been implicated as an important factor in Sr/Ca ratios, particularly in this genus [*Cohen et al.*, 2004; *Goodkin et al.*, 2005], so I compared the annual Sr/Ca ratios with the annual growth rates of the individual corals (Figure 13 a–c). None of the individual corals had a significant relationship between Sr/Ca and growth rate on an annual basis (Table 6). However, mean growth rates and the mean Sr/Ca ratio are different between corals (Figure 13d, Table 6). An ANOVA (Analysis Of Variance) test for differences in annual means ($df = 2$, $p < 0.001$) and mean annual growth rates ($df = 2$, $p = 0.0071$) supports this conclusion. Note that the

Bartlett's test [*Bartlett*, 1937] for equality of variance was performed before application of the ANOVA test and the result suggests that the Sr/Ca ratios in the three corals agree with the homogeneity-of-variance assumption for the ANOVA test ($n_{AN17} = 16$; $n_{AN18} = 27$; $n_{AN19} = 9$; $p = 0.6650$), though the same test shows that growth rates in the three corals are only moderately consistent with the homogeneity of variance assumption ($n_{AN17} = 16$; $n_{AN18} = 27$; $n_{AN19} = 9$; $p = 0.0310$).

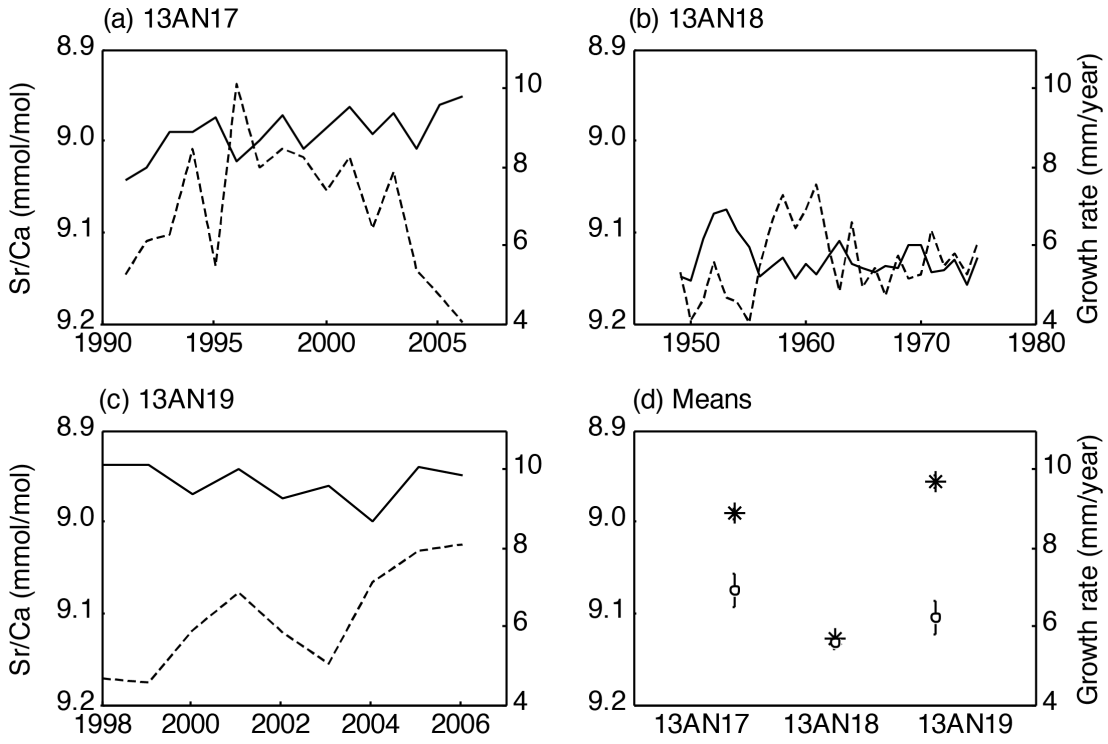

Figure 13. Annual mean Sr/Ca ratios and annual growth rates of modern corals. Growth rates were calculated based on the distance between two successive annual growth markers in Sr/Ca. The dashed lines represent growth rates. The solid lines represent annual mean Sr/Ca values. The asterisks in panel (d) represent mean Sr/Ca. The open circles represent mean growth rates.

Table 6. Annual mean growth rates and Sr/Ca ratios in modern corals.

	AN17	AN18	AN19
Number of years	217	347	124
Mean Sr/Ca (mmol/mol)	8.991±0.006	9.129±0.004	8.957±0.007
Mean Extension rate (mm/year)	6.9±0.4	5.6±0.2	6.2±0.4
Annual Sr/Ca-Extension correlation	0.16	0.32	0.14
p-value	0.55	0.10	0.71

2.4 Discussion

2.4.1 Calibration and Verification of Sr/Ca–SST Calibration

In this study, I applied both the OLS and RMA regression techniques not only to compare the regression equations from different techniques, but also to compare the regression with previous studies. WLS and BWLS techniques were used to explore how the different assumptions of error impact a calibration.

The assumption of no errors in the independent variables distinguishes the OLS technique from the other three regression methods. However, the OLS technique provides similar regressions as the WLS and BWLS techniques because temperature resolution is finer than the errors in the Sr/Ca ratio data. RMA assumes there are errors in the independent variables, but it presumes equal error variances, which does not hold for the available modern gridded SST data and it produced significantly different slopes. The WLS technique, which uses weighted errors, gives a similar Sr/Ca–SST relationship as the OLS method, indicating that the standard

practice of OLS calibration is reasonable considering the variable weight of errors in SSTs and Sr/Ca data.

The major advantage of the WLS regression has over other techniques is its ability to handle data of varying quality. However, one shared disadvantage of OLS and WLS techniques is that they are sensitive to the effects of outliers. If potential outliers are not investigated and dealt with appropriately, they can have a negative impact on the precision of parameter estimations. We suggest a more robust BWLS technique to test how the potential outliers affect the calibrations.

The BWLS technique gives an estimate of the range of regression results when sampled multiple times from a population with the same error statistics as the data. The average regression represents an overall regression for this technique. Additionally, the 25% of the data left out of each regression calculation provides regression-independent data to assess reconstruction errors. For each iteration of the regression, the derived Sr/Ca–SST slope is applied to these regression-independent data and the calculated SSTs compared to instrumental SST. 95% of the monthly SST reconstructions are within ±0.4°C of the instrumental temperature, providing a 95% confidence level that can be assigned to a reconstructed temperature. This is essentially the same as the expected 2 sigma analytical precision based on the coral reference standard. The regression of Sr/Ca–SST anomalies provides monthly SST reconstructions that have relatively large errors, ±0.8°C at the 95% confidence level.

I chose the BWLS regression based on the mean-centered Sr/Ca ratio of all three modern corals to reconstruct the temperature because the WLS calibration

technique accounts for unequal errors in both the dependent and independent variables and thus provides the best estimation of the underlying Sr/Ca–SST relationship. Additionally, the use of three individual coral heads in the regression minimizes the potential influence of differences between coral colonies in a population to get a result that is more appropriately applicable to an individual chosen from the population at random e.g., a sub-fossil coral washed ashore. It is not ideal to calibrate solely on seasonal cycles, but the low signal-to-noise ratio of the anomaly data and the fact that similar results are obtained with the anomaly data, provide confidence that the multi-coral mean-centered calibration is appropriate for reconstructing both seasonal and interannual temperatures.

I reconstructed SST in modern periods based on the BWLS regression and compared the results with the instrumental SST data to test the calibration. Figure 14 shows the reconstructed SST and the gridded SST during the same periods in modern corals. These data include a signal from the seasonal cycle (Figure 15) and interannual variability in the anomalies from the seasonal cycle (Figure 16). The average absolute difference between the reconstructed monthly temperature and the actual temperature is 0.48°C. With the annual cycle removed, the average absolute difference between the monthly reconstructed and instrumental SST is 0.84°C. For the climatological annual cycles, the average difference in terms of temperature is 0.25°C. These results suggest that *D. strigosa* corals can be reliably used to reconstruct seasonal temperature variability within 0.25°C and, with greater uncertainty, can be used to reconstruct SST anomalies.

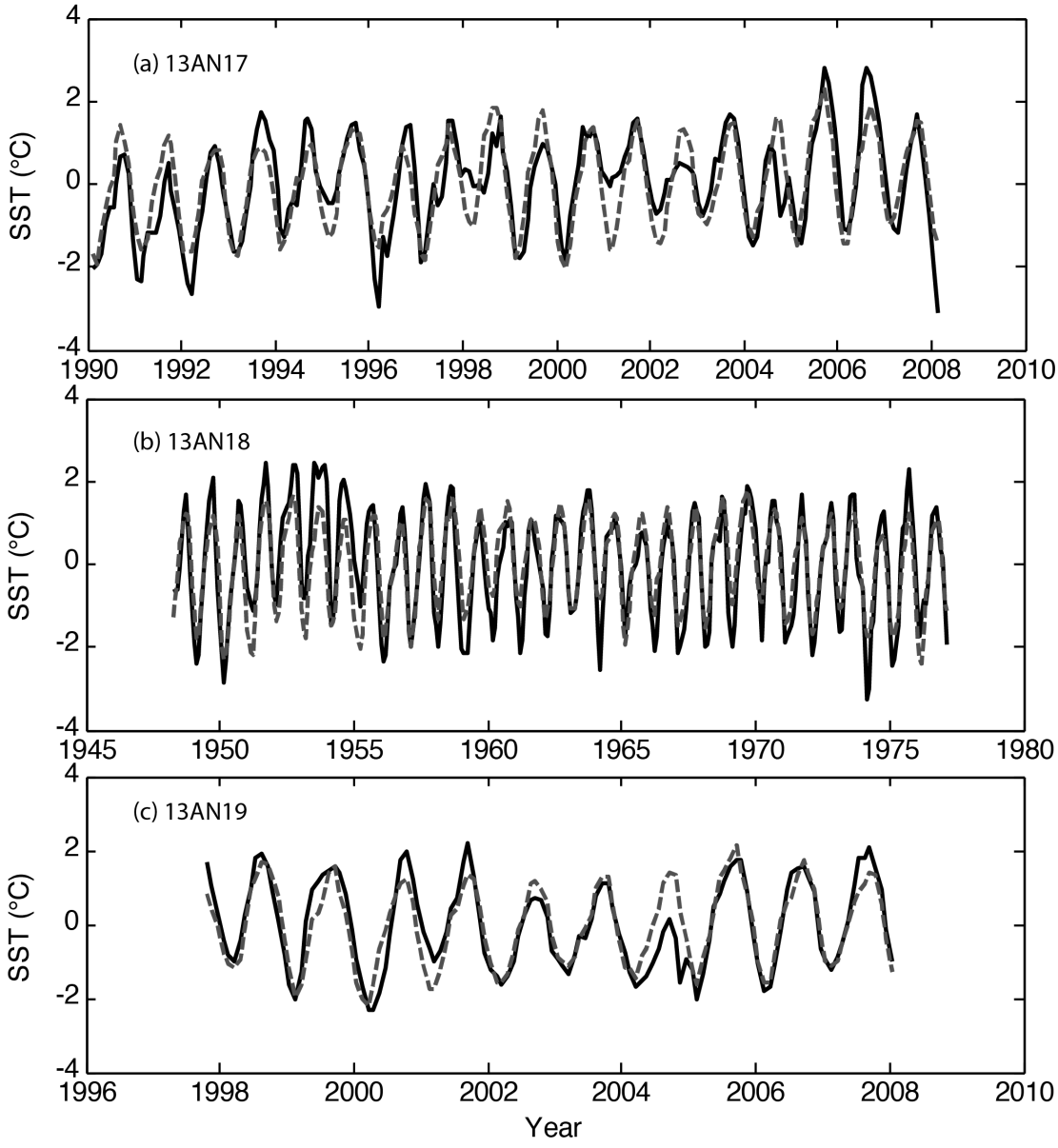

Figure 14. Reconstructed SST anomalies from modern corals by using centered-Sr/Ca records. From top to bottom the panels represent coral 13AN17, 13AN18, and 13AN19, respectively. Solid lines represent the reconstructed SST. Dashed lines represent the gridded SST.

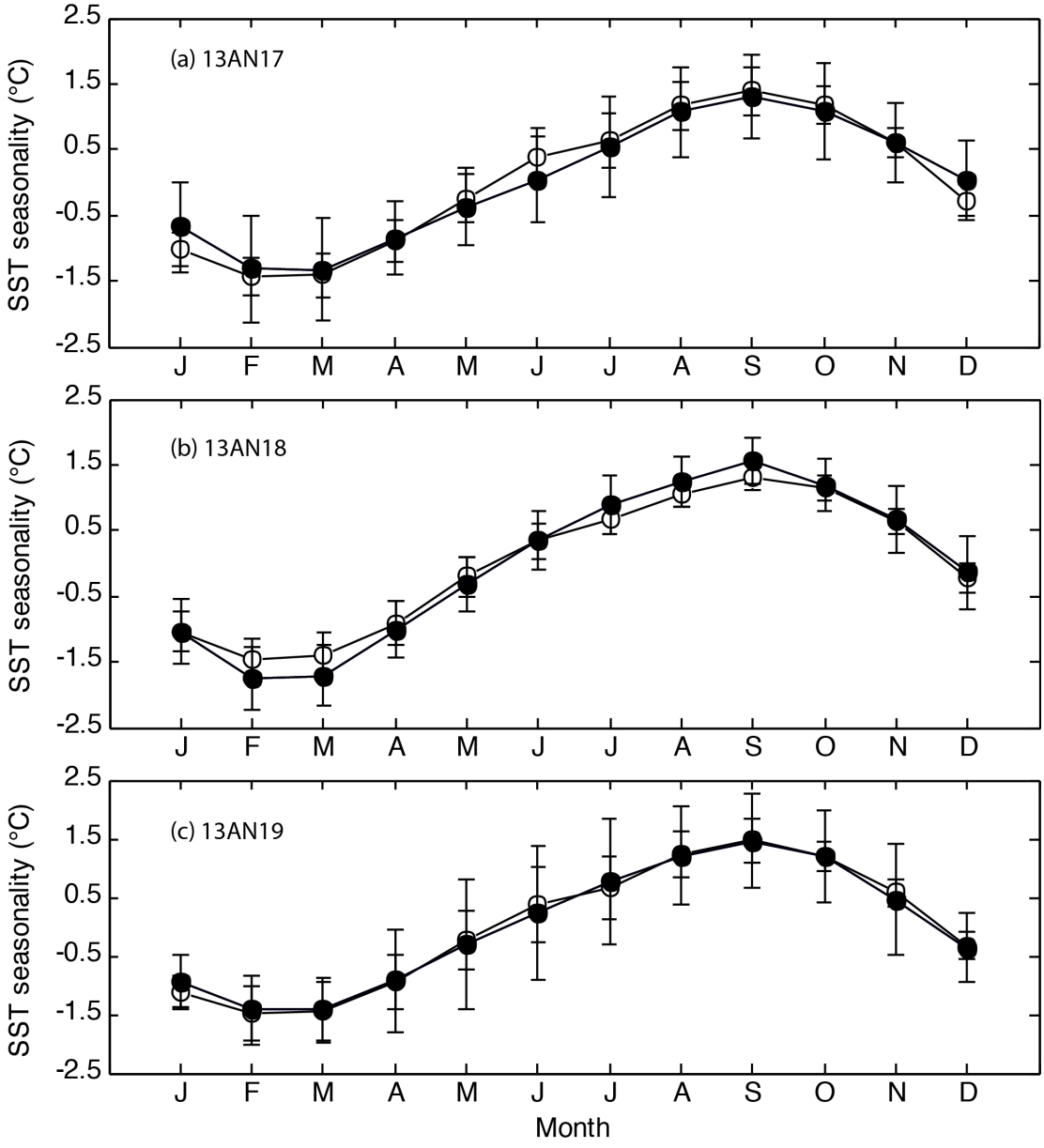

Figure 15. Average monthly Sr/Ca and instrumental SST in modern corals. Black lines with closed circles represent coral Sr/Ca seasonality and black lines with open circles represent instrumental SST seasonality during the growth periods of modern corals. All error bars represent 2SE.

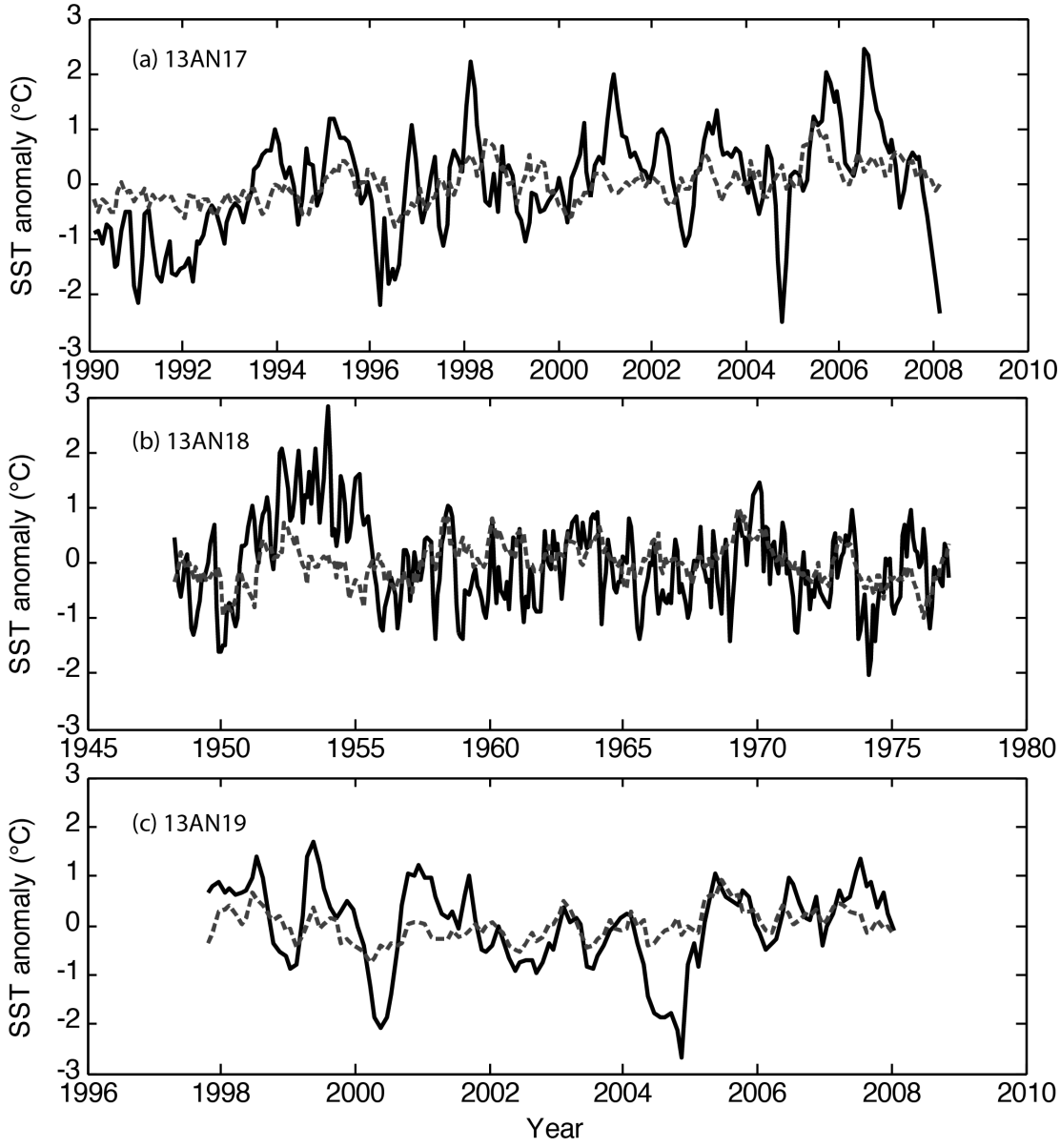

Figure 16. Monthly reconstructed SST anomalies and instrumental gridded SST anomalies in modern corals. Solid lines represent reconstructed SST anomalies derived from coral Sr/Ca and dashed lines represent instrumental gridded SST during the growth periods of modern corals.

2.4.2 Inter-colony Offsets of Mean Sr/Ca Ratios

The corals in this study have different mean Sr/Ca ratios that cannot be explained by differences in mean temperature at the time of coral growth according to

the gridded temperature data. The difference in temperatures during the periods that these modern corals grew only explains 12% of the mean Sr/Ca ratio variability, based on the Sr/Ca−SST sensitivity of the BWLS calibration equation.

Although many studies have demonstrated the consistency of Sr/Ca ratios among coral colonies [*DeLong et al.*, 2007; *Stephans et al.*, 2004], there is some evidence that different coral colonies growing near each other can have colony-specific offsets in mean Sr/Ca ratios [*de Villiers* et al., 1994]. Potential factors that might cause such offsets include species effects, growth rate differences, water depth differences and seawater Sr/Ca differences [*Goodkin et al.*, 2005; *Pfeiffer et al.*, 2008; *Shen et al.*, 1996]. Mean Sr/Ca ratio offsets in the corals from this study cannot be explained by species effects because all the samples are the same species. This leaves growth rate differences, water depth differences, and/or seawater Sr/Ca differences as possible explanations for the observed mean variation.

Steep thermal gradients in the reef surface waters can potentially cause mean Sr/Ca differences between corals growing at different depths on the same reef. Depth-dependent changes in skeletal carbon isotopic composition provide a way to assess if differences in depth can explain the Sr/Ca data. Hermatypic corals contain photosynthesizing endosymbiotic zooxanthellae that exhibit light-driven $\delta^{13}C$ variations [*Guilderson and Schrag*, 1999]. During photosynthesis the zooxanthellae preferentially utilize ^{12}C in the production of organic matter, leaving the carbon pool that is utilized by the coral to construct its skeleton enriched in ^{13}C [*Weber and Woodhead*, 1970]. This fractionation results in an observed $\delta^{13}C$ depth distribution where individuals from shallower depths (exposed to more light and undergoing

higher photosynthetic rates) have higher ^{13}C content. This mechanism is not likely to explain the mean shift of the Sr/Ca ratio in our modern corals because $\delta^{13}C$ values in 13AN17 and 13AN19 are significantly lower than in 13AN18, suggesting that corals 13AN17 and 13AN19 lived in deeper water depths than 13AN18. If this were the case, I would expect higher Sr/Ca ratios in 13AN17 and 13AN19 due to colder temperatures, but the opposite pattern is found. 13AN17 and 13AN19 have lower Sr/Ca ratios than 13AN18.

It has been demonstrated that, within a single species, slow-growing colonies or parts of colonies can have higher Sr/Ca ratios [*de Villiers et al.*, 1994; *Goodkin et al.*, 2005]. Several explanations have been developed to explain the mechanisms. For example, *Ferrier-Pagès et al.* [2002] concluded that kinetic effects may explain the influence of growth rate after their culture study demonstrated that coral skeletons tend to have high Sr/Ca ratios at low calcification rates. They hypothesized that this is due to increased uptake of Sr relative to Ca, but *Allison et al.* [2011] argue that the *Ferrier-Pagès et al.* [2002] experimental design could not distinguish a change in Sr uptake in response to differences in calcification rates. *Elderfield et al.* [1996] hypothesized that a Rayleigh fractionation model explains how the growth rate affects the uptake of trace metals by corals. *Gaetani et al.* [2011] also used a similar approach to verify that Rayleigh fractionation plays an important role in coral elemental composition, although these results are not universally accepted [*Allison et al.* 2011].

Even though there is no significant relationship between monthly Sr/Ca and growth rate in each coral colony, it is possible that the mean shift of the growth rates

in these three modern corals are responsible for the mean shift of the Sr/Ca ratios (Table 6). Considering the relatively high Sr/Ca ratios and relatively low growth rates in coral 13AN18 compared to other modern corals, I conclude that the difference in growth rates may contribute to the mean shifts in Sr/Ca ratios. This is consistent with previous studies that suggest slower growing colonies have higher Sr/Ca ratios [*de Villiers et al.*, 1994; *Goodkin et al.*, 2005].

Another possibility is that the difference in mean Sr/Ca is due to differences in seawater Sr/Ca ratios [*de Villiers*, 1999; *de Villiers et al.*, 1994]. Constant seawater Sr/Ca has been assumed in coral Sr/Ca paleothermometry [*Corrège*, 2006], but in costal reef zones, seawater Sr/Ca ratio may vary [*Smith et al*., 2006]. The reef crest is subject to high wave energy and has a specific fauna, dominated by encrusting calcareous algae rather than coral [*Done*, 1982]. This environment has different ratios of calcite (low Sr/Ca) versus aragonite (high Sr/Ca) producing organisms than the back or fore reef environments where corals make up the primary carbonate structures [*Done*, 1999]. The seawater in the fore reef region, which is farthest away from the shore, can have relative higher Sr/Ca value due to upwelling, which transport high Sr to the surface. Considering the fact that these modern corals were collected from a beach deposit, they may come from different reef zones, which may have different seawater Sr/Ca ratios.

2.5 Conclusions

In this study, I assess four different calibration regression methods and conclude that the standard practice of OLS regression is reasonable given the distribution of error between the geochemistry and instrumental temperature data. I recommend a more robust WLS regression and a BWLS regression to estimate the confidence intervals of the slopes. My calibration using *D. strigosa* is similar to previous calibrations using this species from other sites, suggesting that climate calibrations from my study are widely applicable to this species where it is distributed. In addition, my results indicate that whereas significant mean differences among individuals at the study site were observed, seasonal and interannual temperature variability can still be distinguished using the skeletal geochemistry of *D. strigosa*.

References

Allison, N., A. A. Finch, J. M. Webster, and D. A. Clague (2007), Palaeoenvironmental records from fossil corals: the effects of submarine diagenesis on temperature and climate estimates, *Geochimica et Cosmochimica Acta*, *71*(19), 4693-4703.

Allison, N., I. Cohen, A. A. Finch, and J. Erez (2011), Controls on Sr/Ca and Mg/Ca in scleractinian corals: The effects of Ca-ATPase and transcellular Ca channels on skeletal chemistry, *Geochimica et Cosmochimica Acta*, *75*(21), 6350-6360.

Amador, J. A. (1998), A climatic feature of the tropical Americas: The trade wind easterly jet, *Topicos Meteorologicos Oceanogrraficos*, *5*(2), 1-13.

Atwater, B. F., Z. Fuentes, R. B. Halley, U. S. ten Brink, and M. P. Tuttle (2014), Effects of 2010 Hurricane Earl amidst geologic evidence for greater overwash at Anegada, British Virgin Islands, *Advances in Geosciences*, *38*(38), 21-30.

Atwater, B. F., U. S. ten Brink, M. Buckley, R. S. Halley, B. E. Jaffe, A. M. López-Venegas, E. G. Reinhardt, M. P. Tuttle, S. Watt, and Y. Wei (2012), Geomorphic and stratigraphic evidence for an unusual tsunami or storm a few centuries ago at Anegada, British Virgin Islands, *Natural Hazards*, *63*(1), 51-84.

Bartlett, M. S. (1937), Properties of sufficiency and statistical test, *Proceedings of the Royal Statistical Society*, *160*(901), 268-282.

Bevington, P. R., and D. K. Robinson (1969), *Data reduction and error analysis for the physical sciences*, McGraw-Hill New York.

Budd, A. F., H. Fukami, N. D. Smith, and N. Knowlton (2012), Taxonomic classification of the reef coral family Mussidae (Cnidaria: Anthozoa: Scleractinia), *Zoological Journal of the Linnean Society*, *166*(3), 465-529.

Cahyarini, S. Y., M. Pfeiffer, O. Timm, W.-C. Dullo, and D. G. Schönberg (2008), Reconstructing seawater $\delta^{18}O$ from paired coral $\delta^{18}O$ and Sr/Ca ratios: Methods, error analysis and problems, with examples from Tahiti (French Polynesia) and Timor (Indonesia), *Geochimica et Cosmochimica Acta*, *72*(12), 2841-2853.

Cavalli-Sforza, L. L., and A. W. Edwards (1967), Phylogenetic Analysis Models and Estimation Procedures, *American Journal of Human Genetics*, *19*(3 Part 1), 233.

Chahine, M. T. (1992), The hydrological cycle and its influence on climate, *Nature*, *359*(6394), 373-380.

Chérubin, L. M., and P. L. Richardson (2007), Caribbean current variability and the influence of the Amazon and Orinoco freshwater plumes, *Deep Sea Research Part I: Oceanographic Research Papers*, *54*(9), 1451-1473.

Clarke, M. R. B. (1980), The reduced major axis of a bivariate sample, *Biometrika*, *67*(2), 441-446.

Cohen, A. L., S. R. Smith, M. S. McCartney, and J. van Etten (2004), How brain corals record climate: an integration of skeletal structure, growth and chemistry of Diploria labyrinthiformis from Bermuda, *Marine Ecology Progress Series*, *271*, 147-158.

Collins, M., R. Knutti, J. Arblaster, J.-L. Dufresne, T. Fichefet, P. Friedlingstein, X. Gao, W.J. Gutowski, T. Johns, G. Krinner, M. Shongwe, C. Tebaldi, A.J. Weaver, and M. Wehner, 2013: Long-term climate change: Projections, commitments and irreversibility. In *Climate Change 2013: The Physical Science Basis. Contribution of Working Group I to the Fifth Assessment Report of the Intergovernmental Panel on Climate Change*. T.F. Stocker, D. Qin, G.-K. Plattner, M. Tignor, S.K. Allen, J. Doschung, A. Nauels, Y. Xia, V. Bex, and P.M. Midgley, Eds. Cambridge University Press, 1029-1136.

Corrège, T. (2006), Sea surface temperature and salinity reconstruction from coral geochemical tracers, *Palaeogeography, Palaeoclimatology, Palaeoecology*, *232*(2-4), 408-428.

Crowley, T. J., T. M. Quinn, and W. T. Hyde (1999), Validation of coral temperature calibrations, *Paleoceanography*, *14*(5), 605-615.

Czaja, A., P. Van der Vaart, and J. Marshall (2002), A diagnostic study of the role of remote forcing in tropical Atlantic variability, *Journal of Climate*, *15*(22), 3280-3290.

Davis, D., and K. Oldfield (2003), Archaeological Reconnaissance of Anegada, British Virgin Islands, *Journal of Caribbean Archaeology*(4), 1-11.

Davis, J. C. (2002), *Statistics and Data Analysis in Geology*, 3rd ed., Wiley, New York.

de Villiers, S. (1999), Seawater strontium and Sr/Ca variability in the Atlantic and Pacific oceans, *Earth and Planetary Science Letters*, *171*(4), 623-634.

de Villiers, S., G. T. Shen, and B. K. Nelson (1994), The Sr/Ca-temperature relationship in coralline aragonite: Influence of variability in (Sr/Ca)seawater and skeletal growth parameters, *Geochimica et Cosmochimica Acta*, *58*(1), 197-208.

Delcroix, T., L. Gourdeau, and C. Hénin (1998), Sea surface salinity changes along the Fiji‐Japan shipping track during the 1996 La Niña and 1997 El Niño period, *Geophysical research letters*, *25*(16), 3169-3172.

Delcroix, T., M. J. McPhaden, A. Dessier, and Y. Gouriou (2005), Time and space scales for sea surface salinity in the tropical oceans, *Deep Sea Research Part I: Oceanographic Research Papers*, *52*(5), 787-813.

DeLong, K. L., T. M. Quinn, and F. W. Taylor (2007), Reconstructing twentieth-century sea surface temperature variability in the southwest Pacific: A replication study using multiple coral Sr/Ca records from New Caledonia, *Paleoceanography*, *22*(4), PA4212.

Dessier, A., and J. R. Donguy (1994), The sea surface salinity in the tropical Atlantic between 10 S and 30 N—Seasonal and interannual variations (1977–1989), *Deep Sea Research Part I: Oceanographic Research Papers*, *41*(1), 81-100.

Done, T. J. (1982), Patterns in the distribution of coral communities across the central Great Barrier Reef, *Coral Reefs*, *1*(2), 95-107.

Done, T. J. (1999), Coral community adaptability to environmental change at the scales of regions, reefs and reef zones, *American Zoologist*, *39*(1), 66-79.

Dunne, R. P., and B. E. Brown (1979), *Some aspects of the ecology of reefs surrounding Anegada, British Virgin Islands*, Smithsonian Inst.

Elderfield, H., C. Bertram, and J. Erez (1996), A biomineralization model for the incorporation of trace elements into foraminiferal calcium carbonate, *Earth and Planetary Science Letters*, *142*(3), 409-423.

Esper, J., E. R. Cook, and F. H. Schweingruber (2002), Low-frequency signals in long tree-ring chronologies for reconstructing past temperature variability, *Science*, *295*(5563), 2250-2253.

Fairbanks, R. G., M. N. Evans, J. L. Rubenstone, R. A. Mortlock, K. Broad, M. D. Moore, and C. D. Charles (1997), Evaluating climate indices and their geochemical proxies measured in corals, *Coral Reefs*, *16*(1), S93-S100.

Fallon, S. J., M. T. McCulloch, R. van Woesik, and D. J. Sinclair (1999), Corals at their latitudinal limits: laser ablation trace element systematics in *Porites* from Shirigai Bay, Japan, *Earth and Planetary Science Letters*, *172*(3–4), 221-238.

Ferrier-Pagès, C., F. Boisson, D. Allemand, and E. Tambutté (2002), Kinetics of strontium uptake in the scleractinian coral Stylophora pistillata, *Marine ecology Progress Series*, *245*, 93-100.

Fitch, W. M., and E. Margoliash (1967), Construction of phylogenetic trees, *Science*, *155*(760), 279-284.

Folland, C. K., T. N. Palmer, and D. E. Parker (1986), Sahel rainfall and worldwide sea temperatures, 1901-85, *Nature*, *320*(6063), 602-607.

Gaetani, G. A., A. L. Cohen, Z. Wang, and J. Crusius (2011), Rayleigh-based, multi-element coral thermometry: a biomineralization approach to developing climate proxies, *Geochimica et Cosmochimica Acta*, *75*(7), 1920-1932.

Gagan, M. K., G. B. Dunbar, and A. Suzuki (2012), The effect of skeletal mass accumulation in Porites on coral Sr/Ca and $\delta^{18}O$ paleothermometry, *Paleoceanography*, *27*(1), PA1203.

Gagan, M. K., L. Ayliffe, J. Beck, J. Cole, E. Druffel, R. Dunbar, and D. Schrag (2000), New views of tropical paleoclimates from corals, *Quaternary Science Reviews*, *19*(1), 45-64.

Gagan, M. K., L. K. Ayliffe, D. Hopley, J. A. Cali, G. E. Mortimer, J. Chappell, M. T. McCulloch, and M. J. Head (1998), Temperature and surface-ocean water balance of the mid-Holocene tropical western Pacific, *Science*, *279*(5353), 1014-1018.

Gallup, C. D., D. M. Olson, R. L. Edwards, L. M. Gruhn, A. Winter, and F. W. Taylor (2006), Sr/Ca-Sea surface temperature calibration in the branching Caribbean coral *Acropora palmata*, *Geophysical Research Letters*, *33*(3), L03606.

George, S. E., and M. A. Saunders (2001), North Atlantic Oscillation impact on tropical north Atlantic winter atmospheric variability, *Geophysical Research Letters*, *28*(6), 1015-1018.

Giry, C., T. Felis, M. Kölling, and S. Scheffers (2010), Geochemistry and skeletal structure of *Diploria strigosa*, implications for coral-based climate reconstruction, *Palaeogeography, Palaeoclimatology, Palaeoecology*, *298*(3-4), 378-387.

Giry, C., T. Felis, M. Kölling, D. Scholz, W. Wei, G. Lohmann, and S. Scheffers (2012), Mid-to late Holocene changes in tropical Atlantic temperature seasonality and interannual to multidecadal variability documented in

southern Caribbean corals, *Earth and Planetary Science Letters*, *331*, 187-200.
Goodkin, N. F., K. A. Hughen, and A. L. Cohen (2007), A multicoral calibration method to approximate a universal equation relating Sr/Ca and growth rate to sea surface temperature, *Paleoceanography*, *22*(1), PA1214.
Goodkin, N. F., K. A. Hughen, A. L. Cohen, and S. R. Smith (2005), Record of Little Ice Age sea surface temperatures at Bermuda using a growth-dependent calibration of coral Sr/Ca, *Paleoceanography*, *20*(4), PA4016.
Guilderson, T. P., and D. P. Schrag (1999), Reliability of coral isotope records from the Western Pacific Warm Pool: A comparison using age‐optimized records, *Paleoceanography*, *14*(4), 457-464.
Hansen, J., R. Ruedy, M. Sato, and K. Lo (2010), GLOBAL SURFACE TEMPERATURE CHANGE, *Reviews of Geophysics*, *48*(4), RG4004.
Hastenrath, S., and L. Heller (1977), Dynamics of climatic hazards in northeast Brazil, *Quarterly Journal of the Royal Meteorological Society*, *103*(435), 77-92.
Hetzinger, S., M. Pfeiffer, W.-C. Dullo, E. Ruprecht, and D. Garbe-Schönberg (2006), Sr/Ca and $\delta^{18}O$ in a fast-growing *Diploria strigosa* coral: Evaluation of a new climate archive for the tropical Atlantic, *Geochemistry, Geophysics, Geosystems*, *7*(10), Q10002.
Hirabayashi, S., Y. Yokoyama, A. Suzuki, Y. Kawakubo, Y. Miyairi, T. Okai, and S. Nojima (2013), Coral growth-rate insensitive Sr/Ca as a robust temperature recorder at the extreme latitudinal limits of *Porities*, *Geochemical Journal*, *47*(3), e1-e5.
Hoerling, M. P., J. W. Hurrell, and T. Xu (2001), Tropical origins for recent North Atlantic climate change, *Science*, *292*(5514), 90-92.
Hu, Z.-Z., and B. Huang (2007), The Predictive Skill and the Most Predictable Pattern in the Tropical Atlantic: The Effect of ENSO, *Monthly Weather Review*, *135*(5), 1786-1806.
Huber, W., A. Von Heydebreck, H. Sültmann, A. Poustka, and M. Vingron (2002), Variance stabilization applied to microarray data calibration and to the quantification of differential expression, *Bioinformatics*, *18*(suppl 1), S96-S104.
Hurrell, J. W. (1995), Decadal trends in the North Atlantic Oscillation: regional temperatures and precipitation, *Science*, *269*(5224), 676-679.
Jones, P. D., T. J. Osborn, and K. R. Briffa (2001), The Evolution of Climate Over the Last Millennium, *Science*, *292*(5517), 662-667.
Karl, T. R., and K. E. Trenberth (2003), Modern global climate change, *science*, *302*(5651), 1719-1723.
Kerr, R. A. (2001), The tropics return to the climate system, *Science*, *292*(5517), 660-661.
Kilbourne, K. H., T. M. Quinn, F. W. Taylor, T. Delcroix, and Y. Gouriou (2004), El Niño-Southern Oscillation-related salinity variations recorded in the skeletal geochemistry of a *Porites* coral from Espiritu Santo, Vanuatu, *Paleoceanography*, *19*(4), PA4002.

Kilbourne, K. H., T. M. Quinn, R. Webb, T. Guilderson, J. Nyberg, and A. Winter (2008), Paleoclimate proxy perspective on Caribbean climate since the year 1751: Evidence of cooler temperatures and multidecadal variability, *Paleoceanography*, *23*(3), PA3220.

Kinder, T. H., G. W. Heburn, and A. W. Green (1985), Some aspects of the Caribbean circulation, *Marine Geology*, *68*(1), 25-52.

Knutson, T. R., J. L. McBride, J. Chan, K. Emanuel, G. Holland, C. Landsea, I. Held, J. P. Kossin, A. Srivastava, and M. Sugi (2010), Tropical cyclones and climate change, *Nature Geoscience*, *3*(3), 157-163.

Le Bec, N., A. Julliet-Leclerc, T. Corrège, D. Blamart, and T. Delcroix (2000), A coral $\delta^{18}O$ record of ENSO driven sea surface salinity variability in Fiji (south-western tropical Pacific), *Geophysical Research Letters*, *27*(23), 3897-3900.

Li, Y., F. Wang, and W. Han (2013), Interannual sea surface salinity variations observed in the tropical North Pacific Ocean, *Geophysical Research Letters*, *40*(10), 2194-2199.

Maes, C. (2000), Salinity variability in the equatorial Pacific Ocean during the 1993–98 period, *Geophysical Research Letters*, *27*(11), 1659-1662.

Malmgren, B. A., A. Winter, and C. Deliang (1998), El Niño--Southern Oscillation and North Atlantic Oscillation Control of Climate in Puerto Rico, *Journal of Climate*, *11*(10), 2713.

Marshall, et al. (2001), North Atlantic climate variability: phenomena, impacts and mechanisms, *International Journal of Climatology*, *21*(15), 1863-1898.

Maupin, C. R., T. M. Quinn, and R. B. Halley (2008), Extracting a climate signal from the skeletal geochemistry of the Caribbean coral Siderastrea siderea, *Geochemistry, Geophysics, Geosystems*, *9*(12), Q12012.

McConnell, M. C., R. C. Thunell, L. Lorenzoni, Y. Astor, J. D. Wright, and R. Fairbanks (2009), Seasonal variability in the salinity and oxygen isotopic composition of seawater from the Cariaco Basin, Venezuela: Implications for paleosalinity reconstructions, *Geochemistry, Geophysics, Geosystems*, *10*(6), Q06019.

McCulloch, M. T., M. K. Gagan, G. E. Mortimer, A. R. Chivas, and P. J. Isdale (1994), A high-resolution Sr/Ca and $\delta^{18}O$ coral record from the Great Barrier Reef, Australia, and the 1982–1983 El Niño, *Geochimica et Cosmochimica Acta*, *58*(12), 2747-2754.

McDermott, F. (2004), Palaeo-climate reconstruction from stable isotope variations in speleothems: a review, *Quaternary Science Reviews*, *23*(7), 901-918.

McGregor, H. V., and M. K. Gagan (2003), Diagenesis and geochemistry of *Porites* corals from Papua New Guinea: Implications for paleoclimate reconstruction, *Geochimica et Cosmochimica Acta*, *67*(12), 2147-2156.

Moore, W. S., and J. F. Todd (1993), Radium isotopes in the Orinoco Estuary and eastern Caribbean Sea, *Journal of Geophysical Research: Oceans (1978–2012)*, *98*(C2), 2233-2244.

Müller-Karger, F., C. McClain, T. Fisher, W. Esaias, and R. Varela (1989), Pigment distribution in the Caribbean Sea: Observations from space, *Progress in Oceanography*, *23*(1), 23-64.

Neelin, J. D., D. S. Battisti, A. C., Hirst, F. F. Jin, Y. Wakata, T. Yamagata, and S. E. Zebiak (1998), ENSO theory, *Journal of Geophysical Research: Oceans (1978-2012)*, *103*(C7), 14261-14290.

Paillard, D., L. Labeyrie, and P. Yiou (1996), Macintosh Program performs time-series analysis, *Eos, Transactions American Geophysical Union*, *77*(39), 379-379.

Peterson, L. C., G. H. Haug, K. A. Hughen, and U. Röhl (2000), Rapid changes in the hydrologic cycle of the tropical Atlantic during the last glacial, *Science*, *290*(5498), 1947-1951.

Pfeiffer, M., W.-C. Dullo, J. Zinke, and D. Garbe-Schönberg (2008), Three monthly coral Sr/Ca records from the Chagos Archipelago covering the period of 1950–1995 A.D.: reproducibility and implications for quantitative reconstructions of sea surface temperature variations, *International Journal of Earth Sciences*, *98*(1), 53-66.

Quinn, T. M., and D. E. Sampson (2002), A multiproxy approach to reconstructing sea surface conditions using coral skeleton geochemistry, *Paleoceanography*, *17*(4), 1062.

Ren, L., B. K. Linsley, G. M. Wellington, D. P. Schrag, and O. Hoegh-Guldberg (2002), Deconvolving the $\delta^{18}O$ seawater component from subseasonal coral 18O and Sr/Ca at Rarotonga in the southwestern subtropical Pacific for the period 1726 to 1997, *Geochimica et Cosmochimica Acta*, *67*(9), 1609-1621.

Reverdin, G., E. Kestenare, C. Frankignoul, and T. Delcroix (2007), Surface salinity in the Atlantic Ocean (30 S–50 N), *Progress in Oceanography*, *73*(3), 311-340.

Reynolds, R. W., T. M. Smith, C. Liu, D. B. Chelton, K. S. Casey, and M. G. Schlax (2007), Daily high-resolution-blended analyses for sea surface temperature, *Journal of Climate*, *20*(22), 5473-5496.

Rogers, J. C. (1988), Precipitation variability over the Caribbean and tropical Americas associated with the Southern Oscillation, *Journal of Climate*, *1*(2), 172-182.

Ropelewski, J. A., and M. S. Halpert (1987), Global and regionsl scale precipitation patterns associated with the El Niño/southern oscillation phenomena, *Monthly Weather Review*, *115*(1606-1626).

Saenger, C., A. L. Cohen, D. W. Oppo, and D. Hubbard (2008), Interpreting sea surface temperature from strontium/calcium ratios in *Montastrea* corals: Link with growth rate and implications for proxy reconstructions, *Paleoceanography*, *23*(3), PA3102.

Schmidt, M. W., H. J. Spero, and D. W. Lea (2004), Links between salinity variation in the Caribbean and North Atlantic thermohaline circulation, *Nature*, *428*(6979), 160-163.

Schrag, D. P. (1999), Rapid analysis of high-precision Sr/Ca ratios in corals and other marine carbonates, *Paleoceanography*, *14*(2), 97-102.

Shen, C.-C., T. Lee, C.-Y. Chen, C.-H. Wang, C.-F. Dai, and L.-A. Li (1996), The calibration of *D*[Sr/Ca]versus sea surface temperature relationship for *Porites* corals, *Geochimica et Cosmochimica Acta*, *60*(20), 3849-3858.

Shen, C.-C., C.-C. Wu, H. Cheng, R. Lawrence Edwards, Y.-T. Hsieh, S. Gallet, C.-C. Chang, T.-Y. Li, D. D. Lam, and A. Kano (2012), High-precision and high-resolution carbonate ^{230}Th dating by MC-ICP-MS with SEM protocols, *Geochimica et Cosmochimica Acta*, *99*, 71-86.

Smith, R. W. Buddemeier, R. C. Redalje, and J. E. Houck (1979), Strontium-Calcium Thermometry in Coral Skeletons, *Science*, *204*(4391), 404-407.

Smith, J. E., M. Shaw, R. A. Edwards, D. Obura, O. Pantos, E. Sala, S. A. Sandin, S. Smriga, M. Hatay, and F. L. Rohwer (2006), Indirect effects of algae on coral: algae-mediated, microbe-induced coral mortality, *Ecology Letters*, *9*(7), 835-845.

Smith, R. J. (2009), Use and misuse of the reduced major axis for line‐fitting, *American Journal of Physical Anthropology*, *140*(3), 476-486.

Smith, T. M., R. W. Reynolds, T. C. Peterson, and J. Lawrimore (2008), Improvements to NOAA's historical merged land-ocean surface temperature analysis (1880-2006), *Journal of Climate*, *21*(10), 2283-2296.

Solow, A. R., and A. Huppert (2004), A potential bias in coral reconstruction of sea surface temperature, *Geophysical Research Letters*, *31*(6), L06308.

Spence, J. M., M. A. Taylor, and A. A. Chen (2004), The effect of concurrent sea‐surface temperature anomalies in the tropical Pacific and Atlantic on Caribbean rainfall, *International journal of climatology*, *24*(12), 1531-1541.

Stansell, N. D., B. A. Steinman, M. B. Abbott, M. Rubinov, and M. Roman-Lacayo (2013), Lacustrine stable isotope record of precipitation changes in Nicaragua during the Little Ice Age and Medieval Climate Anomaly, *Geology*, *41*(2), 151-154.

Stephans, C. L., T. M. Quinn, F. W. Taylor, and T. Corrège (2004), Assessing the reproducibility of coral‐based climate records, *Geophysical Research Letters*, *31*(18).

Stramma, L., and F. Schott (1999), The mean flow field of the tropical Atlantic Ocean, *Deep Sea Research Part II: Topical Studies in Oceanography*, *46*(1), 279-303.

Swart, P. K., H. Elderfield, and M. J. Greaves (2002), A high-resolution calibration of Sr/Ca thermometry using the Caribbean coral Montastraea annularis, *Geochemistry, Geophysics, Geosystems*, *3*(11), 8402.

Thirumalai, K., A. Singh, and R. Ramesh (2011), A MATLAB™ code to perform weighted linear regression with (correlated or uncorrelated) errors in bivariate data, *Journal of the Geological Society of India*, *77*(4), 377-380.

Trenberth, K. (1999), Conceptual Framework for Changes of Extremes of the Hydrological Cycle with Climate Change, *Climatic Change*, *42*(1), 327-339.

Visbeck, M. H., J. W. Hurrell, L. Polvani, and H. M. Cullen (2001), The North Atlantic Oscillation: past, present, and future, *Proceedings of the National Academy of Sciences of the USA*, *98*(23), 12876-12877.

Wang, B., R. Wu, and R. Lukas (1999), Roles of the western North Pacific wind variation in thermocline adjustment and ENSO phase transition, *Journal of the Meteorological Society of Japan*, *77*, 1-16.

Wang, C. (2002), Atlantic climate variability and its associated atmospheric circulation cells, *Journal of Climate*, *15*(13), 1516-1536.

Wang, C., and D. B. Enfield (2001), The Tropical Western Hemisphere Warm Pool, *Geophysical Research Letters*, *28*(8), 1635-1638.

Wang, C., and D. B. Enfield (2003), A further study of the tropical Western Hemisphere warm pool, *Journal of Climate*, *16*(10), 1476-1493.

Wang, C., S.-K. Lee, and D. B. Enfield (2008), Atlantic Warm Pool acting as a link between Atlantic Multidecadal Oscillation and Atlantic tropical cyclone activity, *Geochemistry, Geophysics, Geosystems*, *9*(5), Q05V03.

Wang, H.-J., R.-H. Zhang, J. Cole, and F. Chavez (1999), El Niño and the related phenomenon Southern Oscillation (ENSO): the largest signal in interannual climate variation, *Proceedings of the National Academy of Sciences of the USA*, *96*(20), 11071-11072.

Watanabe, T., A. Winter, and T. Oba (2001), Seasonal changes in sea surface temperature and salinity during the Little Ice Age in the Caribbean Sea deduced from Mg/Ca and $^{18}O/^{16}O$ ratios in corals, *Marine Geology*, *173*(1–4), 21-35.

Watanabe, T., A. Winter, T. Oba, R. Anzai, and H. Ishioroshi (2002), Evaluation of the fidelity of isotope records as an environmental proxy in the coral Montastraea, *Coral Reefs*, *21*(2), 169-178.

Weber, J. N., and P. M. J. Woodhead (1970), Carbon and oxygen isotope fractionation in the skeletal carbonate of reef-building corals, *Chemical Geology*, *6*, 93-117.

Weber, J. N., and P. M. J. Woodhead (1972), Temperature dependence of oxygen-18 concentration in reef coral carbonates, *Journal of Geophysical Research*, *77*(3), 463-473.

Weber, J. N. (1973), Incorporation of strontium into reef coral skeletal carbonate, *Geochimica et Cosmochimica Acta*, *37*(9), 2173-2190.

Xie, S.-P., and J. A. Carton (2013), Tropical Atlantic Variability: Patterns, Mechanisms, and Impacts, in *Earth's Climate*, pp. 121-142, American Geophysical Union.

Yao, T., L. Thompson, Y. Shi, D. Qin, K. Jiao, Z. Yang, L. Tian, and E. Thompson (1997), Climate variation since the last interglaciation recorded in the Guliya ice core, *Science in China Series D: Earth Sciences*, *40*(6), 662-668.

Yoo, J.-M., and J. A. Carton (1990), Annual and interannual variation of the freshwater budget in the tropical Atlantic Ocean and the Caribbean Sea, *Journal of Physical Oceanography*, *20*(6), 831-845.

York, D., N. M. Evensen, M. L. Martınez, and J. D. B. Delgado (2004), Unified equations for the slope, intercept, and standard errors of the best straight line, *American Journal of Physics*, *72*(3), 367-375.

Zhang, R., and T. L. Delworth (2005), Simulated tropical response to a substantial weakening of the Atlantic thermohaline circulation, *Journal of Climate*, *18*(12), 1853-1860.

Chapter 3: Sub-fossil Coral Study

3.1 Introduction

The Medieval Climate Anomaly (MCA) is a period of scientific interest for understanding climate change over the past 1000 years [*Crowley*, 2000]. Earlier paleoclimate work indicated that the Medieval period was a particularly warm period globally [*Crowley and Lowery*, 2000], although now it is recognized that while the North Atlantic region was considerably warmer than in the late 20th century, Northern Hemisphere average temperatures were not quite as warm [*Mann et al.*, 2009]. Many proxy reconstructions and models have been used in recent decades to explain the mechanisms that promoted the anomalous climate patterns. *Crowley* [2000] suggested that the increased solar irradiance and decreased volcanism might have contributed to warming temperatures. *Cobb et al* [2003] however argued that changes in solar irradiance and volcanism activity did not warm the central tropical Pacific; this was one of many studies that indicated Medieval warming was not uniform. More recently, *Goosse et al*. [2012] proposed that the MCA can be explained by a combination of thermodynamical responses of the climate system to weak changes in solar radiation and a modification of the atmosphere circulation.

The dynamics of the MCA may have been dominated by large-scale climate modes now often associated with interannual variability [*Graham et al.*, 2010; *Mann et al.*, 2009; *Trouet et al.*, 2009]. Results from climate model simulations have suggested that the MCA pattern is consistent with La Niña-like conditions in the tropical Pacific [*Mann et al.*, 2009]. *Graham et al.* [2010] corroborated the La Niña-

like pattern during the MCA using a coupled global climate model. They found that an enhanced zonal Indo-Pacific SST gradient influenced Caribbean and northern tropical Atlantic climate, which is similar to the previously suggested La Niña-like pattern, though with enhanced warming in the west as opposed to cooling in the east [*Graham et al.*, 2010]. *Trouet et al.* [2009] suggested that conditions were more regionally controlled from the Atlantic, via a persistent positive NAO mode that may have strongly influenced the MCA based on a proxy-derived long-term NAO record. Therefore the control of the MCA by either the NAO or Pacific SST gradient remains unclear, but can be addressed by a better understanding of conditions in the Caribbean and tropical North Atlantic during the MCA.

Uncertainties about climate patterns during the MCA are partly due to the limitation of available proxy climate data in space and time [*Cobb et al.*, 2003; *Mann et al.*, 2009]. Many previous paleoclimate studies concerning the MCA have focused on the Pacific Ocean [*Cobb et al.*, 2003; *Mann et al.*, 2005; *Newton et al.*, 2006]. In the Atlantic, most paleoclimate reconstructions of the last millennium have used terrestrial tree rings and ocean sediment cores [*Mann et al.*, 2009], which primarily record variations of hydrological conditions [*Black et al.*, 1999; *Hodell et al.*, 2005]. Existing high-resolution (interannual-to-decadal timescale [*Jones et al.*, 1998]) paleotemperature records from the tropical Atlantic do not extend back far enough to document the MCA [*Black et al.*, 2007; *Haase-Schramm et al.*, 2003; *Kilbourne et al.*, 2008].

Corals living in shallow tropical ocean waters are ideal sources to provide that high-resolution climate information [*Corrège*, 2006]. Sr/Ca and $\delta^{18}O$ derived from

corals have been successfully used to investigate interannual climate variation in the tropics [e.g., *Giry et al*., 2012]. Spectral analysis of coral Sr/Ca and $\delta^{18}O$ provides an approach to study interannual climate conditions especially when instrumental climate data are not available [*Cobb et al.*, 2003; *Giry et al.*, 2012].

In this study, I compare three modern *Diploria strigosa* coral Sr/Ca and $\delta^{18}O$ records with a late-Medieval aged *D. strigosa* coral (13AN13) from Anegada, British Virgin Islands in the northeastern Caribbean. I compare the climate signals recorded in this sub-fossil coral with signals in the modern corals collected from the same site to assess the differences between modern climate in the region and the climate during the late MCA. My assessment includes exploring differences in mean climate state, interannual variability and seasonal cycles between the modern and sub-fossil geochemical records.

These high-resolution climate archives will enable comparison of the modern climate conditions in the tropical North Atlantic with conditions during the late MCA. The reconstruction will extend knowledge of the past climate state over the last 1000 years and contribute to our understanding of the climate system's behavior during the MCA to Little Ice Age (LIA) transition. This improved understanding can be used to validate datasets in hind-cast model experiments for the last 1000 years (e.g., the Paleoclimate Modeling Intercomparison Project community effort [*Schmidt et al*., 2012].

3.2 Methods

3.2.1 Sampling

One sub-fossil coral core was collected in March 2013 approximately 200 meters inland from Soldier Point, on the island of Anegada (18.76 °N, 64.34 °W, Figure 1) and the modern corals were collected from a beach berm deposit on the beach at Soldier Point. The details of sampling the modern corals, 13AN17, 13AN18, and 13AN19, have been described separately (see Chapter 2) and were similar to the treatment of the sub-fossil coral described below. An approximately 8 cm diameter core was drilled from the coral boulder in the field. The core was given sample number 13AN13 and was cut along the direction of growth into approximately 5 mm thick slabs using a tile saw with diamond blade at Chesapeake Biological Laboratory, Solomons, Maryland, USA. The slabs were ultrasonically cleaned in deionized water and air-dried before drilling sub-samples.

Coral slabs were drilled using a computer-controlled micromilling system, equipped with a 0.5-mm diameter carbide steel dental drill bit. Before drilling coral slabs, coral extension rates were estimated by measuring the distance between ten banded couplets. The targeted sampling resolution was 12 samples per year. Sub-samples of skeletal powder were extracted carefully at constant sampling depths (0.5 mm per sub-sample) along the center of the thecal wall, to obtain the best chronology and environmental signal possible [*Giry et al*., 2010].

3.2.2 Coral Sr/Ca and Stable Isotopes

Sr/Ca determinations were made by reacting 150 ± 50 μg coral powder from each sample in 2% trace metal grade nitric acid. Different volumes (2 to 4 mL) of 2% trace metal grade nitric acid were added to each sample to bring the concentration of calcium to ~20 ppm. The elemental ratios were measured on a Perkin Elmer Optima 8300 Inductively Coupled Plasma Optimal Emission Spectrometer (ICP-OES) at Chesapeake Biological Laboratory. Standards with known calcium and strontium concentrations were used to convert instrumental signal intensity to sample concentration. Reference standards were added after each sample to determine instrumental drift during analyses, as described by *Schrag* [1999]. The calcium and strontium concentrations of the reference standards were similar to the samples, with values of ~20 ppm and 400 ppb respectively. An in-house laboratory coral standard from *Orbicella faveolata* (formerly known as *Montastraea faveolata* [*Budd et al.*, 2012]) was used as an independent check of analytical precision. The standard was dissolved in 2% trace metal grade nitric acid to similar calcium concentration as the samples. Analytical precision for the reference standard solution was 0.12% (2σ, 0.011 mmol/mol, n = 4475). Analytical precision for the coral standard solution was 0.26% (2σ; 0.023 mmol/mol, n = 578). The estimated temperature errors due to analytical precision were calculated by applying a Sr/Ca-temperature relationship of 0.048 mmol $mol^{-1}°C^{-1}$ derived from our modern corals, and are 0.23°C and 0.48°C for the reference and coral standard solution, respectively.

Stable isotope analyses of oxygen and carbon were determined by dissolution of 75±25 μg aliquots of powdered monthly samples in phosphoric acid at 75°C in a

Thermo Scientific Kiel IV automated carbonate preparation device connected to a Thermo Scientific MAT 253 mass spectrometer at the Stable Isotope Geosciences Facility at Texas A&M University. Stable isotopes and Sr/Ca ratios were measured using coral powders from the same aliquots, except for samples from coral 13AN19, in which we drilled a new line from the skeleton for stable analysis due to instrument malfunction. All resulting isotope values are reported in the standard δ-notation relative to the Vienna Pee Dee Belemnite (V-PDB) isotope standard. Six analyses of the international isotope standard NBS-19 were determined during analysis of every 40 samples to determine the instrumental precision ±0.12‰. The estimated temperature error due to analytical precision is 0.06°C by applying a $\delta^{18}O$-temperature relationship of $0.192°C^{-1}$ from *Hetzinger* [2006] to the 2σ standard deviation of the NBS-19 standard.

3.2.3 Coral Chronology

The age of this sub-fossil coral was determined by a combination of uranium-series dating and X-radiography. A sub-sample weighing 811 mg was cut from the top section of the coral slab and sent to the High-Precision Mass Spectrometry and Environment Change Laboratory at National Taiwan University for dating via uranium-series isotope ratios. The wet chemistry was performed following *Shen et al.* [2003] and instrumental analysis was performed on a Multicollector-Inductively Coupled Plasma-Mass Spectrometer (MC-ICP-MS) using the *Shen et al*. [2012] method.

X-radiographs taken at the United States Geological Survey in St. Petersburg, Florida were used to document the annual density band couplets for age modeling.

The positions of the coral pieces that have been dated by uranium-series method can also be identified on X-radiographs. *Knutson et al*. [1972] show that individual high-density and low-density paired bands are annual growth sequences. The ages of specific bands can therefore be determined by counting the number of annual bands relative to any horizon that has been radiometrically dated.

For Sr/Ca, the conversion from depth in the core to date was achieved by matching coral Sr/Ca maximum (minimum) values to SST maximum (minimum) values for each annual cycle using AnalySeries software (available through NOAA's National Climate data center at http://www.ncdc.noaa.gov/data-access/paleoclimatology-data/datasets/software) [*Paillard et al*., 1996]. Additional tie points were utilized to match mid-spring and mid-autumn points between Sr/Ca and SST records to maximize alignment between records because coral extension rate is not constant within a year [*DeLong et al.*, 2007; *Swart et al.*, 2002]. This assumes that SST is the primary driver of Sr/Ca seasonal cycles in the coral skeleton, which has been shown previously with an independent age model (derived from alizarin red staining) by *Swart et al*. [2002]. The SST record used for alignment is the 2° × 2° gridded ERSST version 3b data [*Smith et al*., 2008] centered on 19°N, 64°W. The depth-domain Sr/Ca ratios were then resampled to even monthly intervals to enable comparison with monthly SST time series data.

The age-model for the Sr/Ca data was subsequently utilized to determine growth (extension) rates, and to convert the $\delta^{18}O$ depth series to a time series. Annual extension rates were calculated from two successive winters in each annual cycle as defined by the Sr/Ca-derived age model. For $\delta^{18}O$, the conversion from depth in the

core to time was achieved by matching depth-domain $\delta^{18}O$ values to Sr/Ca-derived ages. The depth-domain $\delta^{18}O$ values were then resampled to monthly intervals.

3.2.4 Reconstructing Seawater $\delta^{18}O$ and Salinity

The $\delta^{18}O$ of seawater ($\delta^{18}O_{sw}$) is calculated from coral Sr/Ca and $\delta^{18}O$ data (*McCullough et al* 1994). Changes in $\delta^{18}O_{sw}$ are determined by subtracting the Sr/Ca-derived SST contribution from the coral $\delta^{18}O$ records. Because the intercepts of the $\delta^{18}O$–SST and Sr/Ca–SST relationships are uncertain due to between-colony mean Sr/Ca and $\delta^{18}O$ offsets [*Ren et al.*, 2002], we calculate seawater $\delta^{18}O$ variations from a reference value (i.e., the average Sr/Ca and $\delta^{18}O$ in this case). The change in coral $\delta^{18}O$ ($\Delta\delta^{18}O_{coral}$) can be written as a combination of the change due to temperature ($\Delta\delta^{18}O_{SST}$) and the change due to seawater $\delta^{18}O$ ($\Delta\delta^{18}O_{sw}$):

$$\Delta\delta^{18}O_{coral} = \Delta\delta^{18}O_{SST} + \Delta\delta^{18}O_{sw} \qquad (1)$$

Equation (1) can be transformed to equation (2):

$$\Delta\delta^{18}O_{sw} = \Delta\delta^{18}O_{coral} - \Delta\delta^{18}O_{SST} \qquad (2)$$

The SST components in coral $\delta^{18}O$ were calculated by the following equation [*Hetzinger et al.*, 2006]:

$$\Delta\delta^{18}O_{SST}\,(PDB) = -0.196(\pm 0.007) \times \Delta SST\ (^{\circ}C) \qquad (3)$$

The seawater surface salinity can be estimated by the known relationship between the $\delta^{18}O$ of seawater and the SSS in southwestern Puerto Rico [*Watanabe et al.*, [2001]:

$$\Delta^{18}O_{sw}\,(SMOW) = 0.204(\pm 0.003) \times \Delta SSS\ (psu) \qquad (4)$$

This equation was determined using 20 samples collected between 1991 and 1998 at La Parguera, Puerto Rico, from which both the isotopic values and salinity were

measured [*Watanabe et al*., 2001]. Note that the scale of the seawater $\delta^{18}O$ here is V-SMOW and it is necessary to add –0.27‰ to data on the V-PDB scale to convert between V-PDB and the V-SMOW scales before applying equation (4) to calculate salinity. Sr/Ca-derived SST can be calculated by using the regression equation (5) generated from three modern corals in Chapter 2 of this thesis:

$$\Delta Sr/Ca = -0.048 \times \Delta SST\ (^{\circ}C) \quad (5)$$

In summary, the SSS can be estimated by using the following equation:

$$\Delta SSS\ (psu) = (\Delta\delta^{18}O_{coral} - (0.196 \times (\Delta Sr/Ca)/0.048) + 0.27)/0.204 \quad (6)$$

3.3 Results

3.3.1 Chronology

The X-radiograph of coral 13AN13 reveals annual density banding patterns (Figure 17). The uranium-series dating result suggests that the age of the cut piece from coral 13AN13 was 1330.3 ± 3.0 CE. Density-band counting of the cut piece to the bottom of the coral places the beginning of the coral growth in the 1260s, which falls in the late Medieval period. This core is 53.0 cm long and it represents growth from 1262 to 1347 ± 3 CE (86 years).

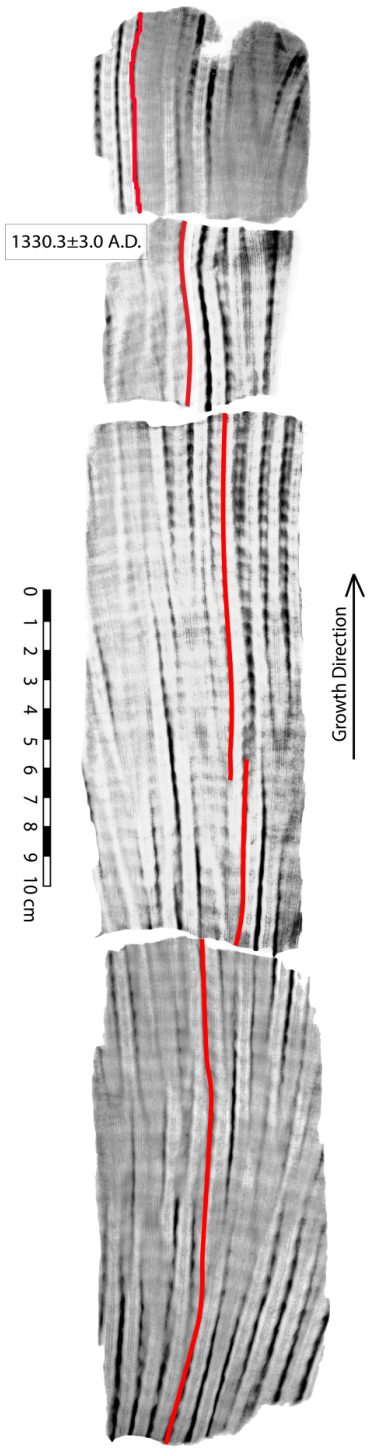

Figure 17. X-radiograph positive prints of slabs of sub-fossil Anegada *D. strigosa* coral 13AN13 reveal the annual density banding patterns. Red lines indicate the position of the micro-sampling transects along the center of the thecal walls. The arrow indicates the growth direction.

3.3.2 Sr/Ca and $\delta^{18}O$ Geochemistry

Both the $\delta^{18}O$ and Sr/Ca time series from the modern coral samples display clear annual cycles, but they do not co-vary at all times and can even display opposite sub-annual variability in some periods (e.g., year 1996-1997 in coral 13AN17, 1957-1958 in coral 13AN18 and 2002-2003 in coral 13AN19 (Figure 18)), indicating that temperature is not the sole driver of the $\delta^{18}O$ signal. The mean Sr/Ca ratio for the modern cores 13AN17, 13AN18, and 13AN19 is 8.99, 9.13, and 8.96 mmol/mol respectively, whereas the mean $\delta^{18}O$ for the same cores is –4.35, –4.24, and –3.93‰ (V-PDB) respectively.

The modern coral $\delta^{18}O$ seasonal cycles lag the Sr/Ca by 1-2 months (Figure 18). The timing of the Sr/Ca seasonal cycle is determined by tying the values to the minimum and maximum temperatures within a year, but the relative phasing of Sr/Ca and $\delta^{18}O$ is not determined by the age model because both Sr/Ca and $\delta^{18}O$ determinations were accomplished on aliquots of the same samples. Note that 13AN19 was excluded from the analysis because only three years of Sr/Ca and $\delta^{18}O$ determinations are available on the same samples, so the relative phasing is not representative.

The monthly coral Sr/Ca data from coral 13AN13 provides 67 years of record for the late Medieval period (Figure 19). The Sr/Ca ratios have a mean value of 9.20 mmol/mol and vary between 9.03 and 9.38 mmol/mol. The coral 13AN13 $\delta^{18}O$ time series (Figure 19) is developed based on the Sr/Ca age model. The $\delta^{18}O$ data range from –4.74 to –3.38‰ (V-PDB), with an average value of –3.98 ±0.01‰ (V-PDB).

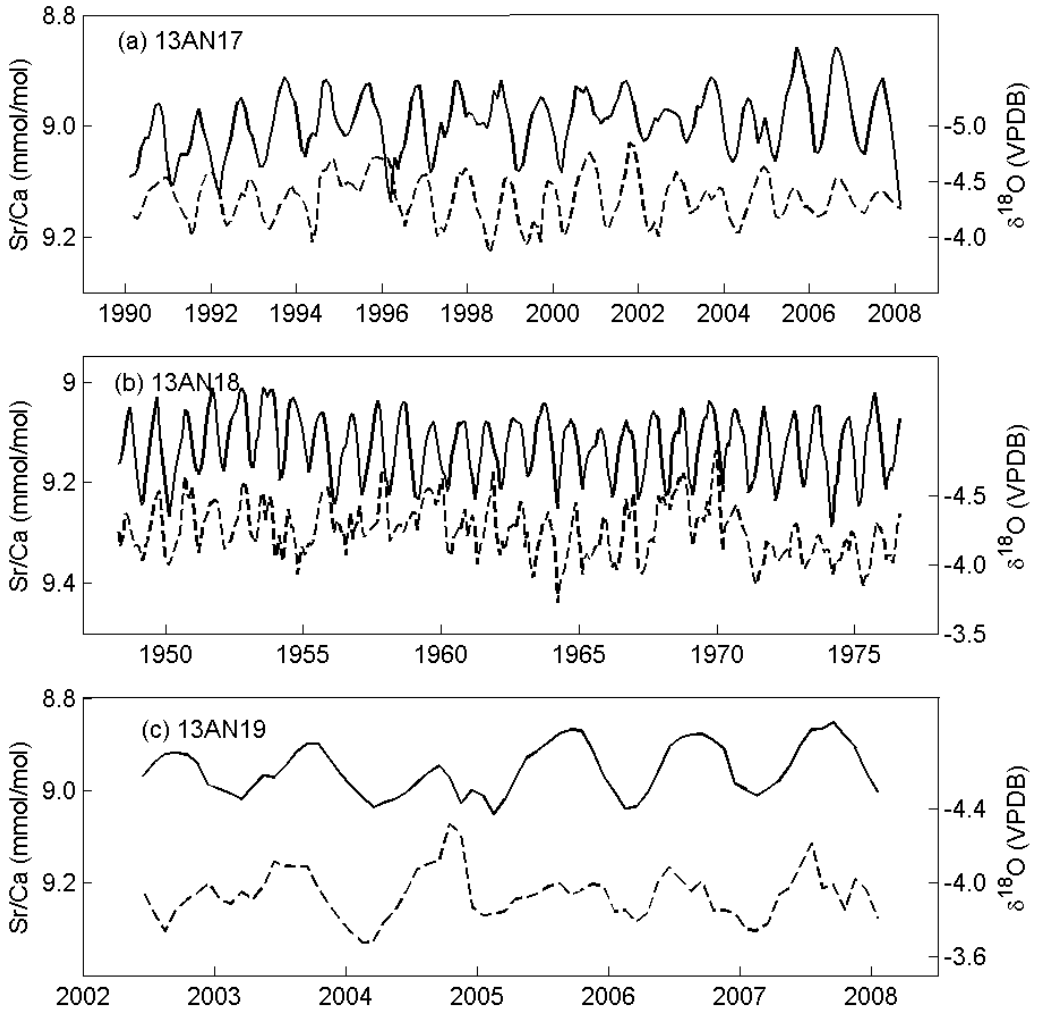

Figure 18. Monthly coral Sr/Ca and $\delta^{18}O$ time series in modern corals. Solid black lines represent monthly Sr/Ca records and dashed lines represent monthly $\delta^{18}O$ records.

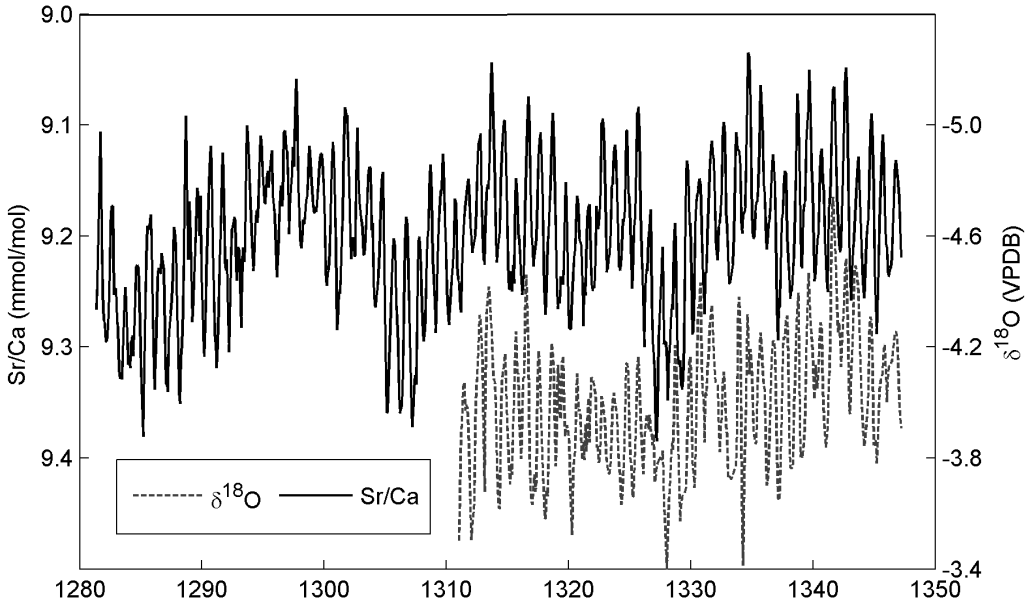

Figure 19. Monthly Anegada sub-fossil coral AN13 Sr/Ca and $\delta^{18}O$ records. The solid line represents the Sr/Ca time series. The dashed line represents $\delta^{18}O$ time series.

Averaging each value for January, February, March, etc., results in a climatological seasonal cycle for each record. The Sr/Ca climatology for 13AN17, 13AN18, and 13AN19 has a seasonal range of 0.13, 0.16, and 0.13 mmol/mol, or 2.7, 3.3 and 2.7°C respectively, with the highest values in February/March and the lowest values in September for all three cores (Figure 20). The $\delta^{18}O$ climatology for 13AN17 and 13AN18 has a seasonal range of 0.39, and 0.29 respectively, with the highest values in March (13AN18) and May (13AN17) and the lowest values in November for both cores (Figure 21).

The comparison of coral Sr/Ca seasonal cycles in our modern and sub-fossil corals suggests similar seasonal temperature patterns throughout the year (Figure 20), although the mean Sr/Ca ratio is 0.18 mmol/mol higher in the sub-fossil coral than

any of the modern corals. This suggests a lower mean temperature (-3.75°C) in the late MCA compared to the modern period based upon the Sr/Ca–SST relationship of -0.048 mmol/mol/°C derived from our modern corals. The $\delta^{18}O$ record is 0.31‰ higher in the sub-fossil record, which if interpreted purely as a temperature difference suggests a temperature drop of 1.58°C during the MCA using the $\delta^{18}O$–SST relationship of -0.196 ‰/°C [*Hetzinger et al.*, 2006]. Interpreting the $\delta^{18}O$ as a combined signal of temperature and seawater $\delta^{18}O$, and assuming the temperature change indicated by the Sr/Ca data is correct, then the $\delta^{18}O$ data indicate a -0.16‰ (SMOW) change in the isotopic composition of the seawater, or -0.76 on the practical salinity scale using a SSS–$\delta^{18}O$ slope of 0.204 ‰/psu [*Watanabe et al.*, 2001] and a $\delta^{18}O$–SST relationship of -0.196 ‰/°C [*Hetzinger et al.*, 2006]. When combined, the mean $\delta^{18}O$ and Sr/Ca data indicate both cooler and less saline conditions during the MCA compared to today.

Unlike the Sr/Ca seasonality, the $\delta^{18}O$ seasonal cycle in the sub-fossil coral is different from the seasonality of the modern corals (Figure 21), indicating a change in the seasonal pattern of seawater isotopic composition. In the sub-fossil coral, the $\delta^{18}O$ seasonal cycle is similar to the Sr/Ca seasonal cycle. Both proxies reach maxima in February and have minima in September. However for modern corals, $\delta^{18}O$ reach maxima later in the spring and reach minima in November. In addition, the range of $\delta^{18}O$ seasonal cycle in the sub-fossil coral is slightly larger than the ranges in modern corals (Figure 21).

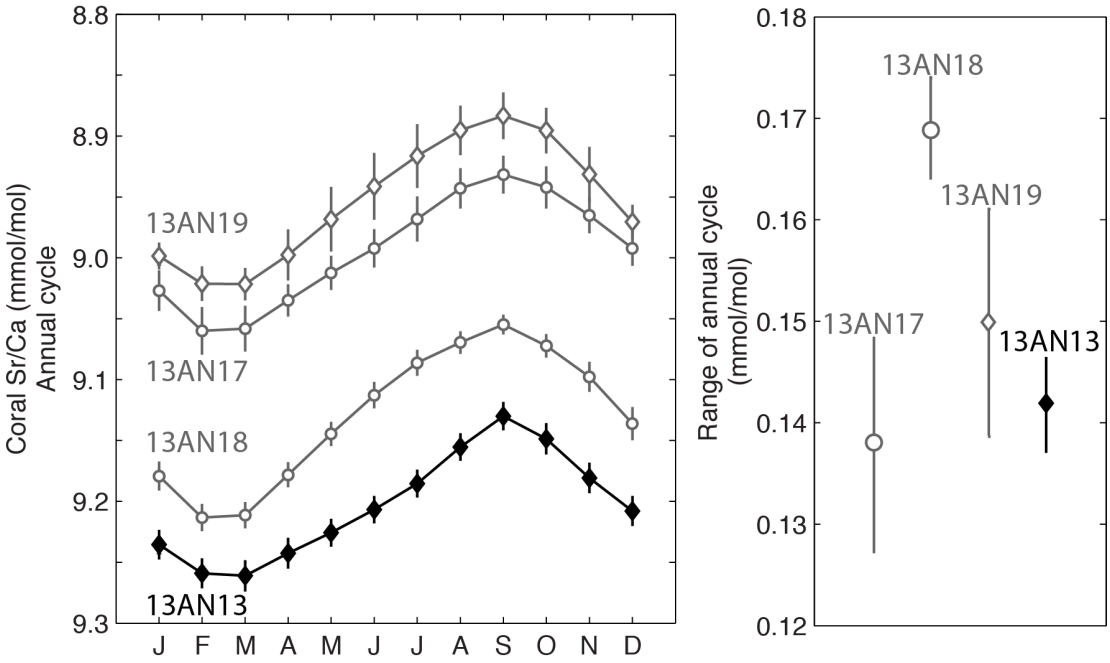

Figure 20. Comparison of seasonal cycles in modern and sub-fossil coral colonies. Grey lines represent modern corals and black lines represent sub-fossil corals. Left panel shows the average monthly Sr/Ca values. The panel on the right shows Sr/Ca average annual ranges in modern and sub-fossil corals. Error bars = ±1 SE.

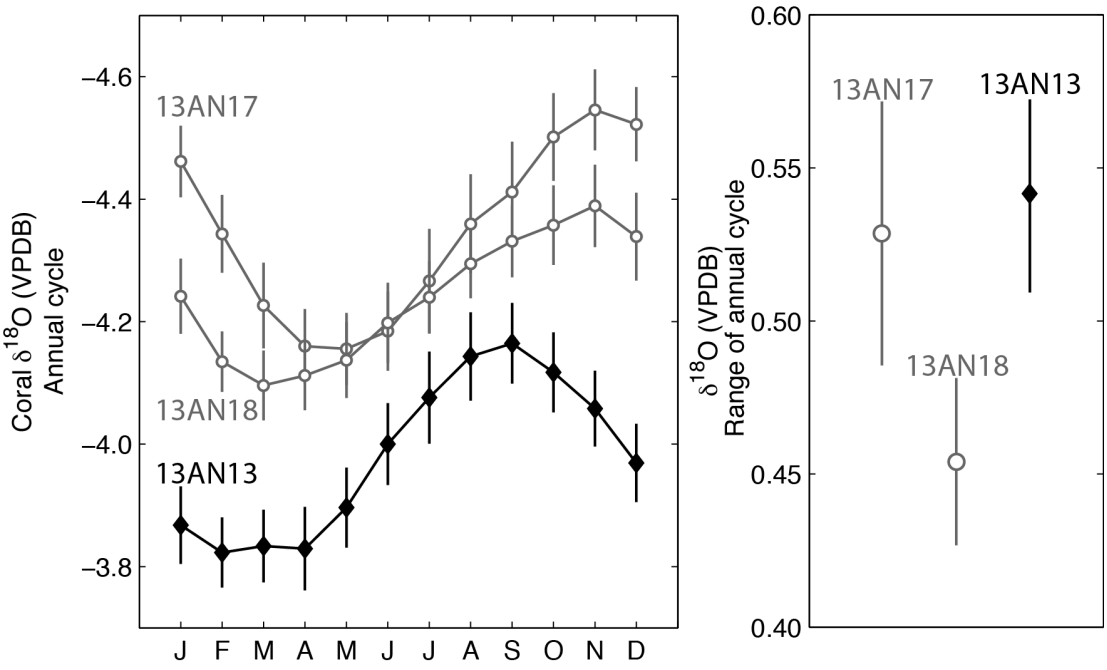

Figure 21. Comparison of average $\delta^{18}O$ annual cycles in modern and sub-fossil coral colonies. Grey lines represent modern corals and black lines represent sub-fossil corals. Left panel shows the average monthly $\delta^{18}O$ values. The panel on the right shows $\delta^{18}O$ average annual ranges in modern and sub-fossil corals. Error bars = ±1 SE.

3.3.3 Reconstructing Temperature from Coral Sr/Ca

Sr/Ca ratio data were converted to temperature by using the relationship of 0.048 mmol/mol/°C derived from our modern corals described in Chapter 2. The reconstructed monthly-resolution SST during the late MCA display clear annual variability with a maximum range of 7.3°C (Figure 22). This range of reconstructed monthly-resolution SST is approximately 1.4 times larger than the range of modern SST in the northeastern Caribbean (1854-2010 CE [*Smith et al.*, 2008]).

I used the annual data to explore the long-term climate variability patterns. The reconstructed annual-resolution SST during the late MCA indicates decadal variability and a slight increasing temperature trend (Figure 22). The range of

reconstructed annual-resolution SST is 1.9 times larger than the range of modern SST in the northeastern Caribbean (1854-2010 CE [*Smith et al.*, 2008]), indicating high temperature fluctuations during the MCA.

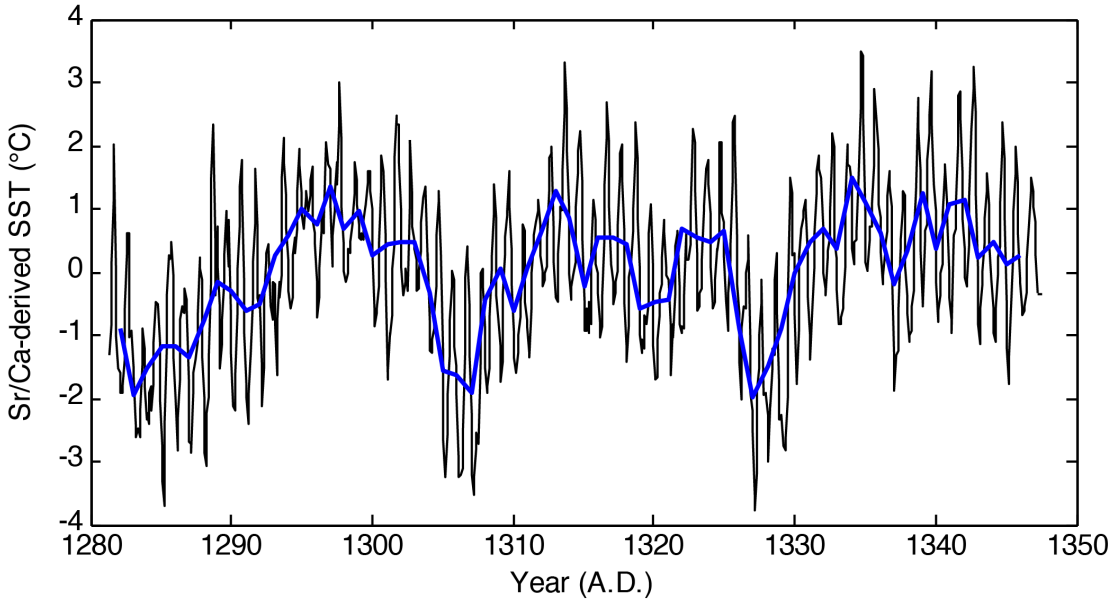

Figure 22. Monthly- and annual- resolution SST reconstructed during the late MCA. SST was reconstructed using Sr/Ca from coral 13AN13 by applying the monthly regression derived from three modern corals. The black line represents monthly SST and the blue line represents the annual SST.

3.3.4 Seawater $\delta^{18}O$ and SSS Variability

The geochemistry data documented in our modern corals reveals that $\delta^{18}O$ and Sr/Ca have different seasonal and interannual patterns (section 3.3.2), indicating that the seasonal $\delta^{18}O$ cycles in these corals are substantially influenced by seawater $\delta^{18}O$ variability since the coral $\delta^{18}O$ signal is driven by both temperature and seawater $\delta^{18}O$, while Sr/Ca ratios are driven primarily by temperature.

The time series of modern seawater $\delta^{18}O$ and SSS anomalies estimated from the equations given in section 3.2.4 are displayed in Figure 23. This analysis requires paired Sr/Ca and $\delta^{18}O$ measured on aliquots of the same sample, and since coral 13AN19 had two independent sampling lines for Sr/Ca and $\delta^{18}O$, I excluded this core from the $\delta^{18}O_{sw}$ and salinity analysis. However, all three corals display apparent seasonal cycles (Figure 21), demonstrating that significant seasonal changes of $\delta^{18}O_{sw}$ occur in the northeastern Caribbean.

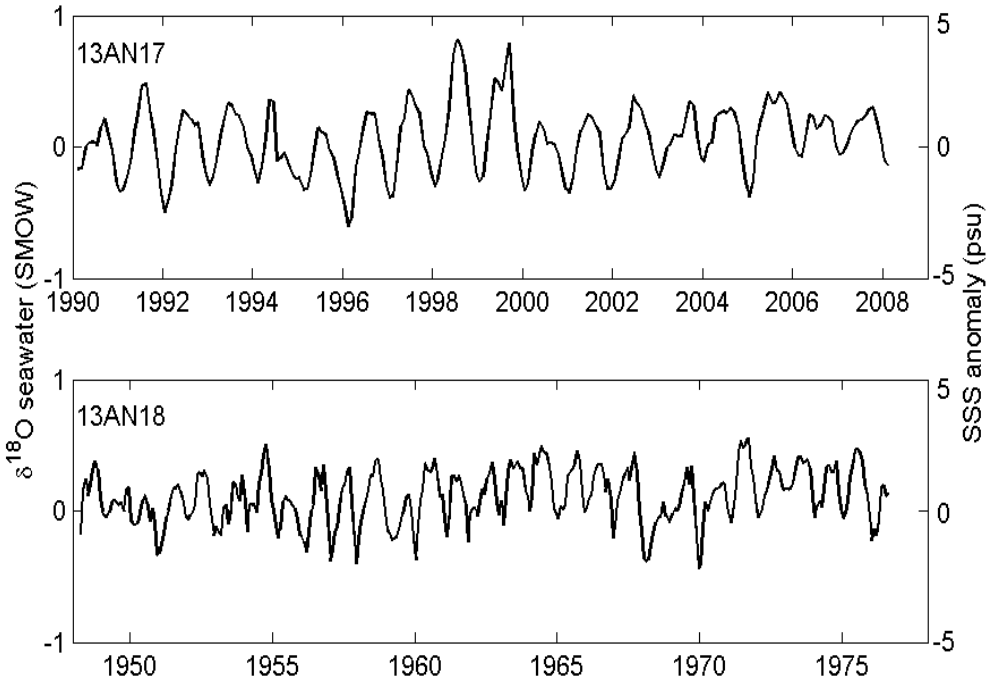

Figure 23. Time series of seawater $\delta^{18}O$ and SSS anomalies derived from two modern corals.

The reconstructed SSS based upon monthly and annual SSS, with the temperature component subtracted from the coral $\delta^{18}O$, shows interannual and decadal variability during the MCA (Figure 24) with a slight decreasing trend.

The seasonal pattern of the reconstructed SSS from the sub-fossil corals has similar phasing to the patterns from the modern corals, but a much smaller amplitude (Figure 25). Annual patterns common to all samples are that salinity increases from March to September and declines September to December. However, the modern corals record lower salinity than the sub-fossil coral at the winter minimum and the salinity ranges in modern corals are greater, indicating there was less seasonal salinity variability during the MCA.

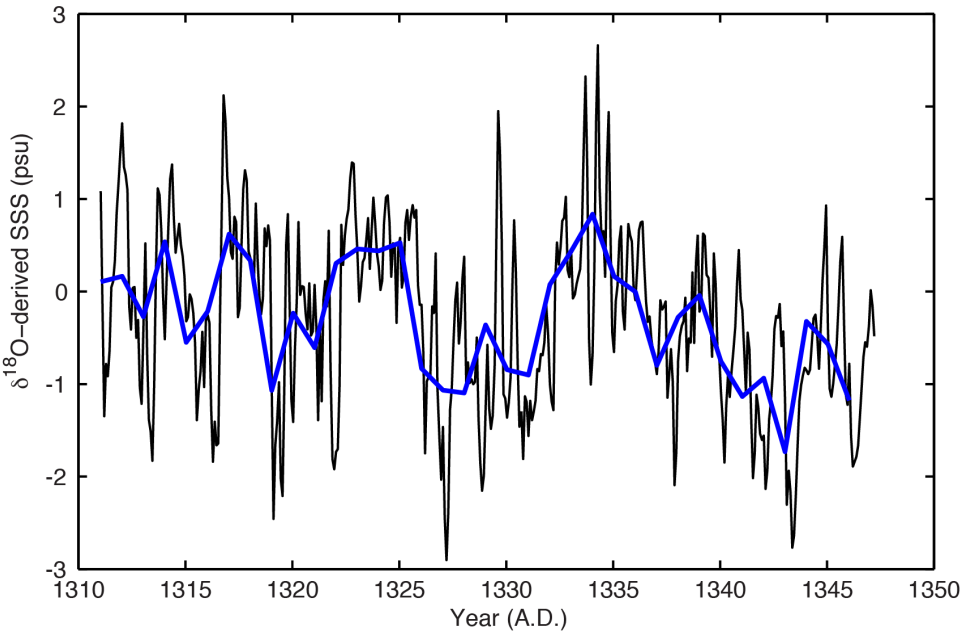

Figure 24. Monthly- and annual- resolution SSS reconstructed during the late MCA. SSS was reconstructed using $\delta^{18}O$ values from coral 13AN13 by subtracting the Sr/Ca-based SST components from the coral $\delta^{18}O$ values. The black line represents monthly SSS and the blue line represents the annual SSS.

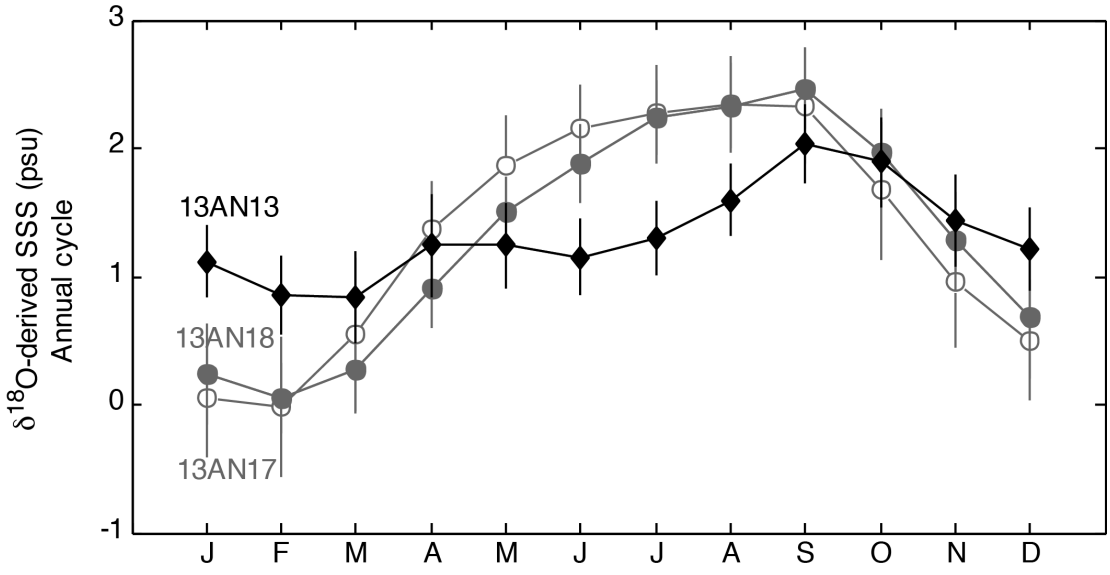

Figure 25. Comparison of reconstructed SSS annual cycles in modern and sub-fossil corals. The grey line with open circles represents SSS reconstructed from modern coral 13AN17. The grey line with closed circles represents SSS reconstructed from modern coral 13AN18. The black line with closed diamonds represents sub-fossil coral 13AN13. Error bars = ± 1 SE.

3.4 Discussion

3.4.1 Cooler and Wetter Northeastern Caribbean during the Late MCA

The Anegada sub-fossil coral Sr/Ca ratio records suggest that the northeastern Caribbean was cooler during the late MCA compared to today. This result is consistent with the idea that the MCA was not a uniformly warm period, but had significant special heterogeneity. The Sr/Ca ratio record in our sub-fossil coral suggests that the temperature was highly variable during the MCA, which may be indicative of increased local upwelling since the samples come from the north coast of a generally east-west trending island subject to the northeast trade winds.

Differences in $\delta^{18}O$ seasonal cycles are also observed in this study. The more stable salinity seasonal pattern documented in the sub-fossil coral suggests a potential change in the location of the salinity front near Anegada during the late MCA. Lower salinities indicated by the geochemical data indicate the northern Caribbean salinity front was north of its current position during the late Medieval period and did not migrate south of Anegada on a seasonal basis as it does today.

It has been suggested that the long-term changes in climate proxies that are recorded during the MCA correspond to a permanent NAO positive phase, a persistent La Niña-like state, or an enhanced Tropical Pacific SST gradient due to warming in the Indo-Pacific Warm Pool [*Graham et al*., 2011; *Mann et al*., 2009; *Trouet et al*., 2009]. The Caribbean Sea is one place where the Pacific-focused modeling work indicates a strong climate signal should be present [*Graham et al*., 2011], but until now, little data was available for verification. The canonical patterns for Atlantic and Pacific climate perturbations (e.g., NAO versus ENSO) leads to different expected climate proxy signatures in the Caribbean (Table 7). In this case, we have evidence for cooler and wetter conditions on average during the MCA, consistent with a modern-day La Niña-state [*Klein et al*., 1999; *Taylor et al*., 2002]. This finding supports the idea that a persistent La Niña-like state dominated the climate system during the MCA, e.g., [Mann et al., 2009, Graham et al, 2011].

Table 7. Canonical or expected response of the Caribbean to specific climate pertubations.

Climate Pattern	Caribbean Precipitation	Caribbean Temperature	Reference
La Niña (modern)	Wetter	Cooler	[*Klein et al.*, 1999; *Taylor et al.*, 2002]
Indo-Pacific SST gradient	Drier	Cooler	[*Graham et al*., 2010]
Positive NAO	Drier	Cooler	[*Czaja and Frankignoul*, 2002]

3.4.2 Interannual Climate Variability in the Modern Period

What was the response of the interannual variability in the tropical Atlantic climate system to the altered mean state? To address this, I compared the interannual signals in instrumental SST records to a modern coral from the region and to sub-fossil corals. Interannual climate signals were picked up though the multi-taper method (MTM) spectral analysis, in which multiple orthogonal windows are applied to time series data for a less biased and more smoothed spectral estimation [*Thomson*, 1982].

Tourre et al. [1999] conducted an analysis of sea level pressure and SST in the Atlantic sector to characterize the interannual to decadal climate variability in the region. They found quasi-biennial modes at 2.2 and 2.7-yr periods related to NAO, a 3.5-yr period peak in spectral power related to ENSO, and a 4.4-yr period band associated with the Atlantic ITCZ location and the cross-equatorial SST gradient (TAV). A spectral analysis of instrumental SST at this study site found significant concentrations of variance at similar frequencies; 2.9, 3.6 and 4.7 years (Figure 26).

Coral Sr/Ca and $\delta^{18}O$ from near-by Puerto Rico also had significant interannual variability concentrated around the 2.3-yr, 3.6-yr, and 4.7-yr periods [*Kilbourne et al*., 2008].

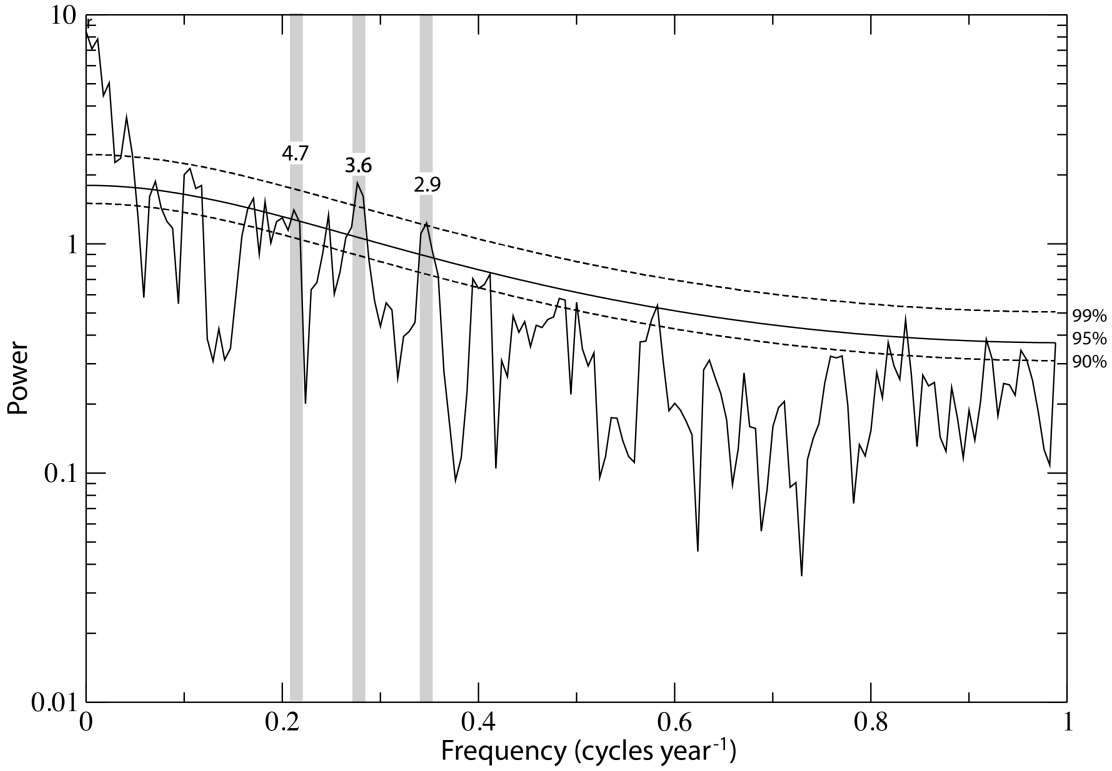

Figure 26. Multi-taper method spectral analysis [*Thomson*, 1982] with a red noise null hypothesis [*Ghil et al*., 2002] of detrended and normalized SST anomalies (1854-2013, 160 years). 90%, 95%, and 99% significance levels are indicated. Numbers on the grey shades indicate high-frequency periods.

The spectral analysis of Sr/Ca time series data measured from coral 13AN13 shows significant 2.2-year power, and a significant power between 4.1- and 5.0-year periods (Figure 27). The 2.2-year period peak in the Atlantic may be related to large-scale sea level pressure variability in the North Atlantic [*Tourre et al.*, 1999],

which is closely linked with NAO [*Visbeck et al.*, 2001]. The existence of a strong quasi-biennial signal in the fossil coral indicates an active NAO pattern during the MCA. Additionally, large amounts of variance in the wide frequency band including the 4.4-yr TAV signal suggest the more Atlantic-driven mode of climate fluctuations during the late MCA [*Tourre et al*., 1999].

The ENSO-associated 3.6-year period detected in the modern temperature records is not found in the sub-fossil records. This is consistent with the analysis of Pacific corals by *Cobb et al*. [2003], who suggested that ENSO activity was weak during the Medieval period. This also suggests that late Medieval interannual climate variability in the Caribbean was driven more by Atlantic climate processes, though the mean state may have been controlled by the state of the tropical Pacific.

Previous studies suggest that Caribbean corals are ideal climate archives for studying the variation of sea surface conditions associated with the Atlantic Multidecadal Oscillation (AMO) [*Hetzinger et al*., 2008; *Kilbourne et al*., 2008]. A significant multidecadal band peaking at 0.03 (i.e., 33.3 years) was detected in the spectral analysis of the Sr/Ca in coral 13AN13 (Figure 27). Interestingly, [*Kobashi et al*., 2010] found a similar ~32-year period of temperature variability over the last millennium by analyzing trapped air in an ice core collected from central Greenland. Multidecadal variability is considered likely due to the instability of the North Atlantic deep water formation and related thermohaline circulation shifts that may have contributed to the MCA [*Esper et al.*, 2002]. However, longer and multiple coral records are needed to further investigate the influence of AMO.

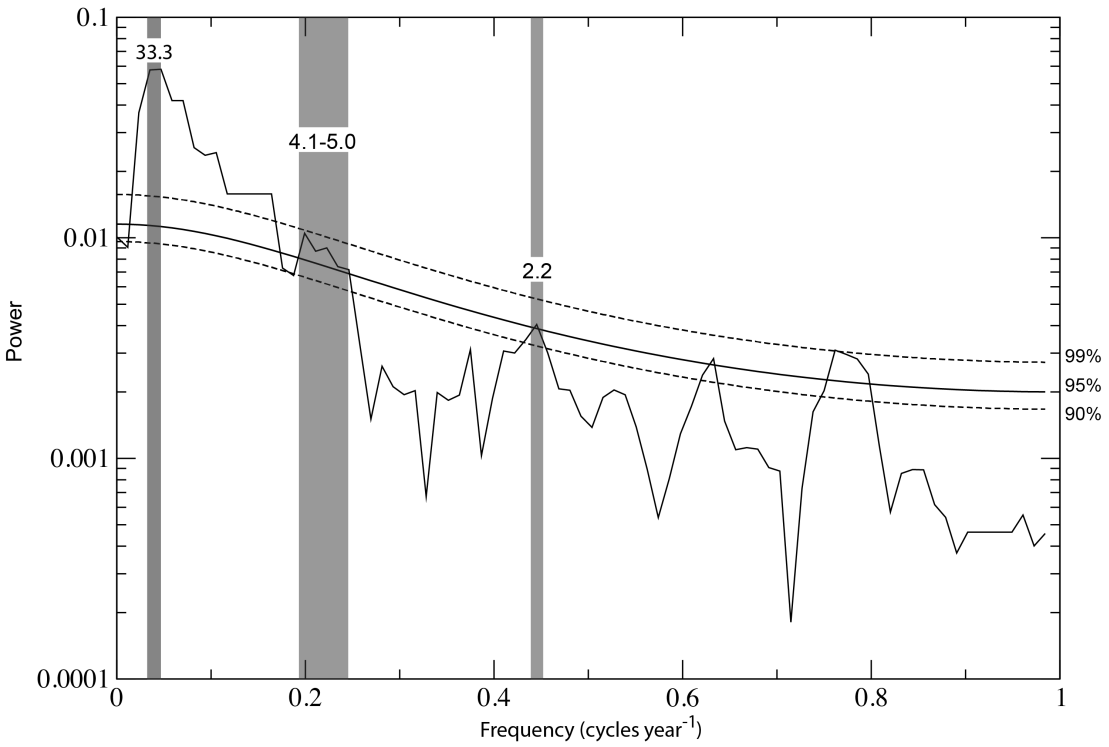

Figure 27. Multi-taper method spectral analysis [*Thomson*, 1982] with a red noise null hypothesis [*Ghil et al.*, 2002] of detrended and normalized sub-fossil coral AN13 Sr/Ca anomalies (of 66 years length). 90%, 95%, and 99% significance levels are indicated. Numbers on the grey shades indicate high-frequency periods.

3.5 Conclusions

My studies indicate a cooler and wetter climate condition in the northeastern Caribbean during the late MCA based on the comparison of geochemistry information in modern and sub-fossil corals, suggesting a La Niña-state climate pattern dominated the long-term climate conditions during the late Medieval period. Combined with the wetter climate condition during the late Medieval period, different $\delta^{18}O$ seasonal cycles in modern and sub-fossil corals indicate a northward expansion of less saline Caribbean surface water during the MCA. On interannual time scale, spectral analyses of the instrumental SST record and modern coral-based climate

records suggest a detectable influence of ENSO and the NAO in the Caribbean. However, no significant ENSO signals were recorded by the Caribbean sub-fossil coral. NAO- and TAV- related signals are found in, suggesting that Atlantic-centered climate processes controlled the Caribbean interannual climate variability during the late MCA. A multidecadal signal is also detected in the sub-fossil coral, but the time series is short with respect to multidecadal variability and longer records are needed to further investigate the influence of AMO in the Caribbean area.

Two other sub-fossil corals that grew at times that overlap the beginning and end of coral 13AN13 are under analysis. They will be used as replicates to support or refute the current conclusions.

References

Black, D. E., L. C. Peterson, J. T. Overpeck, A. Kaplan, M. N. Evans, and M. Kashgarian (1999), Eight centuries of North Atlantic Ocean atmosphere variability, *Science*, *286*(5445), 1709-1713.

Black, D. E., M. A. Abahazi, R. C. Thunell, A. Kaplan, E. J. Tappa, and L. C. Peterson (2007), An 8-century tropical Atlantic SST record from the Cariaco Basin: Baseline variability, twentieth-century warming, and Atlantic hurricane frequency, *Paleoceanography*, *22*(4), PA4204.

Budd, A. F., H. Fukami, N. D. Smith, and N. Knowlton (2012), Taxonomic classification of the reef coral family Mussidae (Cnidaria: Anthozoa: Scleractinia), *Zoological Journal of the Linnean Society*, *166*(3), 465-529.

Cobb, K. M., C. D. Charles, H. Cheng, and R. L. Edwards (2003), El Niño/Southern Oscillation and tropical Pacific climate during the last millennium, *Nature*, *424*(6946), 271-276.

Cook, E. R., J. G. Palmer, and R. D. D'Arrigo (2002), Evidence for a 'Medieval Warm Period' in a 1,100 year tree-ring reconstruction of past austral summer temperatures in New Zealand, *Geophysical Research Letters*, *29*(14), 12-11-12-14.

Corrège, T. (2006), Sea surface temperature and salinity reconstruction from coral geochemical tracers, *Palaeogeography, Palaeoclimatology, Palaeoecology*, *232*(2-4), 408-428.

Crowley, T. J. (2000), Causes of climate change over the past 1000 years, *Science*, *289*(5477), 270-277.

Crowley, T. J., and T. S. Lowery (2000), How warm was the medieval warm period?, *AMBIO: A Journal of the Human Environment*, *29*(1), 51-54.

Czaja, A., and C. Frankignoul (2002), Observed impact of Atlantic SST anomalies on the North Atlantic Oscillation, *Journal of Climate*, *15*(6), 606-623.

DeLong, K. L., T. M. Quinn, and F. W. Taylor (2007), Reconstructing twentieth-century sea surface temperature variability in the southwest Pacific: A replication study using multiple coral Sr/Ca records from New Caledonia, *Paleoceanography*, *22*(4), PA4212.

Esper, J., E. R. Cook, and F. H. Schweingruber (2002), Low-frequency signals in long tree-ring chronologies for reconstructing past temperature variability, *Science*, *295*(5563), 2250-2253.

Giry, C., T. Felis, M. Kölling, and S. Scheffers (2010), Geochemistry and skeletal structure of Diploria strigosa, implications for coral-based climate reconstruction, *Palaeogeography, Palaeoclimatology, Palaeoecology*, *298*(3-4), 378-387.

Giry, C., T. Felis, M. Kölling, D. Scholz, W. Wei, G. Lohmann, and S. Scheffers (2012), Mid-to late Holocene changes in tropical Atlantic temperature seasonality and interannual to multidecadal variability documented in southern Caribbean corals, *Earth and Planetary Science Letters*, *331*, 187-200.

Goosse, H., E. Crespin, S. Dubinkina, M.-F. Loutre, M. E. Mann, H. Renssen, Y. Sallaz-Damaz, and D. Shindell (2012), The role of forcing and internal

dynamics in explaining the "Medieval Climate Anomaly", *Climate dynamics*, *39*(12), 2847-2866.
Graham, N. E., C. M. Ammann, D. Fleitmann, K. M. Cobb, and J. Luterbacher (2010), Support for global climate reorganization during the "Medieval Climate Anomaly", *Climate Dynamics*, *37*(5-6), 1217-1245.
Haase-Schramm, A., F. Böhm, A. Eisenhauer, W. C. Dullo, M. M. Joachimski, B. Hansen, and J. Reitner (2003), Sr/Ca ratios and oxygen isotopes from sclerosponges: Temperature history of the Caribbean mixed layer and thermocline during the Little Ice Age, *Paleoceanography*, *18*(3).
Hetzinger, S., M. Pfeiffer, W.-C. Dullo, E. Ruprecht, and D. Garbe-Schönberg (2006), Sr/Ca and $\delta^{18}O$ in a fast-growing *Diploria strigosa* coral: Evaluation of a new climate archive for the tropical Atlantic, *Geochemistry, Geophysics, Geosystems*, *7*(10), Q10002.
Hetzinger, S., M. Pfeiffer, W.-C. Dullo, N. Keenlyside, M. Latif, and J. Zinke (2008), Caribbean coral tracks Atlantic Multidecadal Oscillation and past hurricane activity, *Geology*, *36*(1), 11-14.
Hodell, D. A., M. Brenner, and J. H. Curtis (2005), Terminal Classic drought in the northern Maya lowlands inferred from multiple sediment cores in Lake Chichancanab (Mexico), *Quaternary Science Reviews*, *24*(12), 1413-1427.
Jones, P. D., K. R. Briffa, T. P. Barnett, and S. F. B. Tett (1998), High-resolution palaeoclimatic records for the last millennium: interpretation, integration and comparison with General Circulation Model control-run temperatures, *The Holocene*, *8*(4), 455-471.
Kilbourne, K. H., T. M. Quinn, R. Webb, T. Guilderson, J. Nyberg, and A. Winter (2008), Paleoclimate proxy perspective on Caribbean climate since the year 1751: Evidence of cooler temperatures and multidecadal variability, *Paleoceanography*, *23*(3), PA3220.
Klein, S. A., B. J. Soden, and N.-C. Lau (1999), Remote Sea Surface Temperature Variations during ENSO: Evidence for a Tropical Atmospheric Bridge, *Journal of Climate*, *12*(4), 917-932.
Knight, J. R. (2009), The Atlantic Multidecadal Oscillation Inferred from the Forced Climate Response in Coupled General Circulation Models, *Journal of Climate*, *22*(7), 1610-1625.
Knutson, D. W., R. W. Buddemeier, and S. V. Smith (1972), Coral Chronometers: Seasonal Growth Bands in Reef Corals, *Science*, *177*(4045), 270-272.
Kobashi, T., K. Kawamura, J. P. Severinghaus, J. M. Barnola, T. Nakaegawa, B. M. Vinther, S. J. Johnsen, and J. E. Box (2011), High variability of Greenland surface temperature over the past 4000 years estimated from trapped air in an ice core, *Geophysical Research Letters*, *38*(21).
Loehle, C. (2007), A 2000-year global temperature reconstruction based on non-treering proxies, *Energy & Environment*, *18*(7), 1049-1058.
Mann, et al. (2009), Global signatures and dynamical origins of the Little Ice Age and Medieval Climate Anomaly, *Science*, *326*(5957), 1256-1260.
Mann, M. E., M. A. Cane, S. E. Zebiak, and A. Clement (2005), Volcanic and solar forcing of the tropical Pacific over the past 1000 years, *Journal of Climate*, *18*(3), 447-456.

McCulloch, M. T., M. K. Gagan, G. E. Mortimer, A. R. Chivas, and P. J. Isdale (1994), A high-resolution Sr/Ca and $\delta^{18}O$ coral record from the Great Barrier Reef, Australia, and the 1982–1983 El Niño, *Geochimica et Cosmochimica Acta*, *58*(12), 2747-2754.

Newton, A., R. Thunell, and L. Stott (2006), Climate and hydrographic variability in the Indo-Pacific Warm Pool during the last millennium, *Geophysical Research Letters*, *33*(19), L19710.

Paillard, D., L. Labeyrie, and P. Yiou (1996), Macintosh Program performs time-series analysis, *Eos, Transactions American Geophysical Union*, *77*(39), 379-379.

Rein, B., A. Lückge, and F. Sirocko (2004), A major Holocene ENSO anomaly during the Medieval period, *Geophysical Research Letters*, *31*(17), L17211.

Ren, L., B. K. Linsley, G. M. Wellington, D. P. Schrag, and O. Hoegh-Guldberg (2002), Deconvolving the 18O seawater component from subseasonal coral 18O and Sr/Ca at Rarotonga in the southwestern subtropical Pacific for the period 1726 to 1997, *Geochim Cosmochim Acta*, *67*(9), 1609-1621.

Schmidt, G., J. Jungclaus, C. Ammann, E. Bard, P. Braconnot, T. Crowley, G. Delaygue, F. Joos, N. Krivova, and R. Muscheler (2011), Climate forcing reconstructions for use in PMIP simulations of the last millennium (v1. 0), *Geoscientific Model Development*, *4*(1).

Schrag, D. P. (1999), Rapid analysis of high‐precision Sr/Ca ratios in corals and other marine carbonates, *Paleoceanography*, *14*(2), 97-102.

Shen, C.-C., H. Cheng, R. L. Edwards, S. B. Moran, H. N. Edmonds, J. A. Hoff, and R. B. Thomas (2003), Measurement of attogram quantities of 231Pa in dissolved and particulate fractions of seawater by isotope dilution thermal ionization mass spectroscopy, *Analytical Chemistry*, *75*(5), 1075-1079.

Shen, C.-C., C.-C. Wu, H. Cheng, R. Lawrence Edwards, Y.-T. Hsieh, S. Gallet, C.-C. Chang, T.-Y. Li, D. D. Lam, and A. Kano (2012), High-precision and high-resolution carbonate ^{230}Th dating by MC-ICP-MS with SEM protocols, *Geochimica et Cosmochimica Acta*, *99*, 71-86.

Smith, T. M., R. W. Reynolds, T. C. Peterson, and J. Lawrimore (2008), Improvements to NOAA's historical merged land-ocean surface temperature analysis (1880-2006), *Journal of Climate*, *21*(10), 2283-2296.

Swart, P. K., H. Elderfield, and M. J. Greaves (2002), A high-resolution calibration of Sr/Ca thermometry using the Caribbean coral Montastraea annularis, *Geochemistry, Geophysics, Geosystems*, *3*(11), 8402.

Taylor, M. A., D. B. Enfield, and A. A. Chen (2002), Influence of the tropical Atlantic versus the tropical Pacific on Caribbean rainfall, *Journal of Geophysical Research: Oceans*, *107*(C9), 3127.

Thomson, D. J. (1982), Spectrum estimation and harmonic analysis, *Proceedings of the IEEE*, *70*(9), 1055-1096.

Trouet, V., J. Esper, N. E. Graham, A. Baker, J. D. Scourse, and D. C. Frank (2009), Persistent positive North Atlantic Oscillation mode dominated the medieval climate anomaly, *Science*, *324*(5923), 78-80.

Visbeck, M. H., J. W. Hurrell, L. Polvani, and H. M. Cullen (2001), The North Atlantic Oscillation: Past, present, and future, *Sciences*, *98*(23), 12876-12877.

Watanabe, T., A. Winter, and T. Oba (2001), Seasonal changes in sea surface temperature and salinity during the Little Ice Age in the Caribbean Sea deduced from Mg/Ca and $^{18}O/^{16}O$ ratios in corals, *Marine Geology*, *173*(1), 21-35.